Tomas Bata University in Zlín
Library

Correlations between the dopant concentration and ion transport properties of plasticized NaCMC-Pectin polyblend electrolyte membranes for electrochemical device applications

Citation

KHELLOUF, Riyadh Abdekadir, Silvie DUŘPEKOVÁ, Vipin CYRIAC, Jaroslav CÍSAŘ, Constantin BUBULINCA, Anežka LENGÁLOVÁ, David ŠKODA, and Vladimír SEDLAŘÍK. Correlations between the dopant concentration and ion transport properties of plasticized NaCMC-Pectin polyblend electrolyte membranes for electrochemical device applications. *Solid State Ionics* [online]. vol. 402, Elsevier, 2023, [cit. 2025-05-27]. ISSN 0167-2738. Available at https://www.sciencedirect.com/science/article/pii/S0167273823002370

DOI

https://doi.org/10.1016/j.ssi.2023.116379

Permanent link

https://publikace.k.utb.cz/handle/10563/1011762

This document is the Accepted Manuscipt version of the article that can be shared via institutional repository.

TBU Publications
Repository of TBU Publications
publikace.k.utb.cz

Correlations between the dopant concentration and ion transport properties of plasticized NaCMC-Pectin polyblend electrolyte membranes for electrochemical device applications

Riyadh Abdekadir Khellouf[a,*], Silvie Durpekova[a], Vipin Cyriac[b], Jaroslav Cisar[a], Constantin Bubulinca[a], Anezka Lengalova[c], David Skoda[a], Vladimír Sedlaríik[a]

[a]*Centre of Polymer Systems, University Institute, Tomas Bata University in Zlin, Tr. T. Bati 5678, 760 01 Zlin, Czech Republic*

[b]*Department of Physics, Manipal Institute of Technology, Manipal Academy of Higher Education, Manipal 576104, Karnataka, India*

[c]*Faculty of Humanities, Tomas Bata University in zlin, Tr. T. Bati 5678, 760 01 Zlin, Czech Republic*

**Corresponding author. E-mail address: khellouf@utb.cz (R.A. Khellouf).*

ABSTRACT

This study explores the structural and electrical properties of sodium carboxymethyl cellulose ($NaCMC$)-pectin (PC)-glycerol-NH_4Br electrolyte films and investigates their potential applications in proton batteries. Plasticized solid polymer electrolyte ($SPEs$) films were fabricated using the solution casting method. The interaction between the salt and polymer blends was verified using Fourier-transform infrared ($FTIR$) analysis. Incorporation of various salt concentrations (up to 25 wt%) was found to enhance the amorphous phase of the polymer blend, as evidenced by X-ray diffraction (XRD) results. Additionally, the decrease in the glass transition temperature, as confirmed by DSC analysis, indicates that the inclusion of both plasticizer and salt contributed to this effect. An electrolyte with 25% wt. of NH_4Br has the highest room temperature conductivity of 4.68×10^{-4} S cm^{-1}. This electrolyte was employed to fabricate the proton battery for energy storage application.

Keywords: Solid biopolymer electrolyte, NaCMC-PC, Glycerol. Proton battery, ionic conductivity

1. Introduction

Owing to the rapid evolution of modern technologies such as portable electronic devices, electric vehicles, and large-scale power sources, it is becoming increasingly essential to develop low-cost and eco-friendly energy storage devices ($ESDs$). In recent years, researchers have utilized conducting membranes in several applications, including supercapacitors, sensors, solar cells, fuel cells, and batteries [**1**]. Generally, most $ESDs$ consist of an anode, cathode, and solid ionconducting electrolyte. From an obvious starting point of view, the electrolyte plays a pivotal role in determining ESD performance. Therefore, the desired properties for an electrolyte to be used in $ESDs$ include high ionic

conductivity ($> 10^{-4}$ S cm^{-1}), high ionic transference number (close to 1), good interfacial contact with the electrodes, high thermal stability, and a wide electrochemical stability window (3-4 V) [**2**]. The most popular electrolytes in the marketplace are liquid electrolytes [**3**]. Nevertheless, inherent issues related to liquid electrolytes, including leakage, thermal runaway, explosion, short circuits, and a low operating window, hinder their optimal performance [**4**]. As a result, researchers have adopted several strategies to enhance the performance of electrolytes by developing solid electrolytes with outstanding properties, such as a wider onset potential range, good ionic conductivity, and stability [**5**].

Since it was first reported in 1973 [**6**] that polyethylene oxide (PEO) can be utilized as an electrolyte, researchers have extensively investigated solid-state polymer electrolytes because of their excellent ionic conductivity, light weight, transparency, film-forming ability, and outstanding mechanical and thermal stability [**7**]. However, synthetic polymer electrolytes are nonbiodegradable and can be noxious and adversely affect the environment. Thus, researchers are continuously exploring biopolymers owing to their biodegradability, nontoxicity, low cost, biocompatibility, and sustainability [**8**]. These properties give biopolymers substantial advantages as appropriate alternatives to synthetic polymers and make them suitable candidates for solid-state electrochemical devices. Several studies have reported that polysaccharides are abundant in nature [**9-11**]. Moreover, they are considered the primary source of biopolymers such as starch, pectin, gum, cellulose, agar, and carrageenan. However, obtaining a high conductivity remains a significant challenge for researchers. Several methods have been adopted to overcome this issue, including cross-linking, copolymerization, plasticizing, and polymer blending [**12**]. Among the techniques already mentioned, polymer blending is considered the most effective technique for improving the electrical properties of polymer electrolytes. It involves a combination of two different types of polymers to provide more complexation sites and enhance the amorphous section of the polymer matrix, thereby improving the segmental motion of the polymer chains as well as facilitating ion mobility and increasing ionic conductivity [**13**].

Pectin (PC) is a biodegradable polymer found primarily in citrus and apple products [**14**]. It has recently attracted considerable attention because of the presence of a large number of hydroxyl groups ($-OH$) in its chemical structure [**15**]. Therefore, blending PC with sodium car-boxymethyl cellulose ($NaCMC$), which shares two main functional groups, carboxylate anion ($COO-$) and hydroxyl $-OH$ in its polymeric backbone, could dramatically help to boost the number of coordination sites, which allows the dissociation of ionic dopants into the polymer matrix and increases the ionic conductivity [**16**]. Because ionic dopants play a significant role in the structure and ionic conductivity of polymer electrolytes, several studies have been carried out on different types of ionic dopant electrolytes, including lithium, sodium, magnesium, and ammonium [**17-19**]. Ammonium salts are considered one of the most promising salts that can be incorporated into biopolymer electrolytes because of their low lattice energy and small cation radius, and more importantly, their good proton donor ability [**20**]. Therefore, protonconducting biopolymer electrolytes based on ammonium salts have shown good ionic conductivities [**21**]. Incorporating glycerol as a plasticizer into the polymer blend significantly enhanced ionic conductivity. This is because glycerol is compatible with a wide range of biopolymers and contains multiple OH groups that act as alternative pathways for ions. In addition, glycerol has a relatively small molecular size, which can disrupt the cohesive forces between polymer chains. This increases the amorphous phase of the polymer electrolytes, which promotes ion dissociation, thereby optimizing the density of the charge carriers [**22**].

According to previous studies, NH_4Br salt has been successfully incorporated into an MC/pectin polymer system blend to synthesize a solid polymer electrolyte. Adam et al. (2022) reported ionic conductivity of 5.9×10^{-5} S cm^{-1} for MC/PC-(EC) blend with 25% (K_3PO_4) [**23**], Dennis et al. (2022)

reported an electrolyte system which is composed of MC/PC/NH_4Cl/ZnO with highest conductivity up to 3.13 × 10-4 S cm^{-1} [**20**]. However, no work has been conducted to improve the ionic conductivity of plasticized NaCMC/PC/NH_4Br polymer electrolyte systems.

The present study uses solution casting technique to enhance the ionic conductivity of a glycerol-plasticized $NaCMC/PC$ blend with different concentrations of NH_4Br salt. The resulting biopolymer blend electrolytes were characterized by $FTIR$, XRD, DSC, TGA, and SEM. In addition, AC impedance analysis was conducted to determine their electrical parameters, and Wagner's DC polarization method was utilized to evaluate the ionic transference number of the electrolytes. Finally, the primary proton battery was fabricated using the electrolyte with the highest conductivity.

2. Experimental

2.1. Materials

Sodium carboxymethyl cellulose ($NaCMC$, $M_w \sim$ 250,000 g mol^{-1}), pectin citrus powder (PC, M_w ~30,000 g mol^{-1}), glycerol ($M_w = 92$ g mol^{-1}), and ammonium bromide (NH_4Br, $M_w = 97.94$ g mol^{-1}) were procured from Sigma-Aldrich, Germany.

The electrodes used in this study for the proton battery were fabricated using the following materials. Zinc metal powder (Zn, $M_w = 65.4$ g mol^{-1}), zinc Sulphate ($ZnSO_4.7H_2O$, $M_w = 161.47$ g mol^{-1}), lead dioxide (PbO_2, $M_w = 239.2$ g mol^{-1}), vanadium pentoxide (V_2O_5, $M_w = 181.9$ g mol^{-1}), polyvinylidene fluoride (PVdF, $M_w \sim$ 534,000 g mol^{-1}) and graphite powder, all were procured from Sigma-Aldrich, Germany.

Table 1 Composition of prepared plasticized $SPEs$ films.

Sample Label	NaCMC/PC(g)	glycerol(g)	NH_4Br (wt%)
C0	3	1	0
C5	2.8	1	5
C10	2.6	1	10
C15	2.4	1	15
C20	2.2	1	20
C25	2	1	25

2.2. Preparation of solid polymer electrolytes

In this study, plasticized $NaCMC - PC$ solid polymer electrolyte films ($SPEs$) with different concentrations (wt%) of NH_4Br salt were prepared using solution casting. $NaCMC$ and PC (3 g) were dissolved in 100 mL distilled water at a weight ratio of 20:80. Subsequently, 1 g glycerol was added to the polymer solution and stirred until a homogeneous solution was obtained. Different NH_4Br concentrations (wt%) of salt were added to the mixture and stirred for 24 h at room temperature, as described previously [**22**]. The compositions of the samples are listed in **Table 1**. The resulting mixtures were poured into separate Petri dishes and allowed to dry at ambient temperature. Finally, the free standing films were peeled off from a glass petri dish and placed inside a desiccator for further characterization.

2.3. Characterization of plasticized $NaCMC/PC$-NH_4Br biopolymer electrolytes

2.3.1. Fourier transform infrared ($FTIR$) spectroscopy

An $FT-IR$ spectrometer ($Nicolet\ iS5$) was utilized to investigate the complexation between the plasticized polymer blend and salt. The analysis was conducted at a resolution of 4 cm^{-1} and wavenumber range of 4000 cm^{-1} – 400 cm^{-1}.

2.3.2. X-ray diffraction (XRD)

X-ray diffraction was employed to study the changes in the crystallinity of the plasticized electrolytes with angular differences between 3° and 90°. The experiments were conducted using a Mini Flex 600 Desk X-ray diffractometer with Cu-Kα radiation ($\lambda = 1.54$ Å) as the X-ray source.

2.3.3. Electrical impedance spectroscopy (EIS)

To investigate the electrical properties of the prepared plasticized $SPEs$, EIS was conducted using Potentiostat/Galvanostat $PG\ STAT$ 128 N equipment at room temperature. Each solid polymer electrolyte film was cut into a circular shape with a diameter of 1.6 cm and then placed between two ion-blocking stainless-steel electrodes, after which an ac signal with an amplitude of 10 mV was applied over a frequency range from 10 to 5 x 105 Hz. Eq. (**1**) was used to calculate the dc conductivity (c) of plasticized biopolymer electrolyte.

$$\sigma = \frac{t}{R_b A} \tag{1}$$

where t represents the thickness of the electrolyte film, R_b is the bulk resistance, and A is the contact area between the polymer electrolyte film and the electrodes. The collected impedance data were transformed into a dielectric format to analyze the dynamic behaviour of the ion/ electrolyte. The real (Ź) and imaginary (Ź) part of the complex impedance were used to determine the real (é) and imaginary (é) parts of the complex permittivity, respectively.

$$\acute{\epsilon} = \frac{\acute{z}}{\omega C_0 \left(\acute{Z}^2 + \acute{Z}^2\right)} \tag{2}$$

$$\acute{\epsilon} = \frac{\acute{z}}{\omega C_0 \left(\acute{Z}^2 + \acute{Z}^2\right)} \tag{3}$$

where ω represents the angular frequency derived from $2\pi f$, and C_0 stands for the vacuum capacitance. Additionally, the real (M') and imaginary (M') parts of the complex modulus were calculated as follows:

$$M' = \frac{\epsilon'}{(\epsilon'^2 + \epsilon''^2)} \quad (4)$$

$$M'' = \frac{\epsilon''}{(\epsilon'^2 + \epsilon''^2)} \quad (5)$$

The tangent loss was evaluated using the following equation:

$$'an\delta = \frac{\epsilon''}{\epsilon'} = \frac{Z'}{Z''} \quad (6)$$

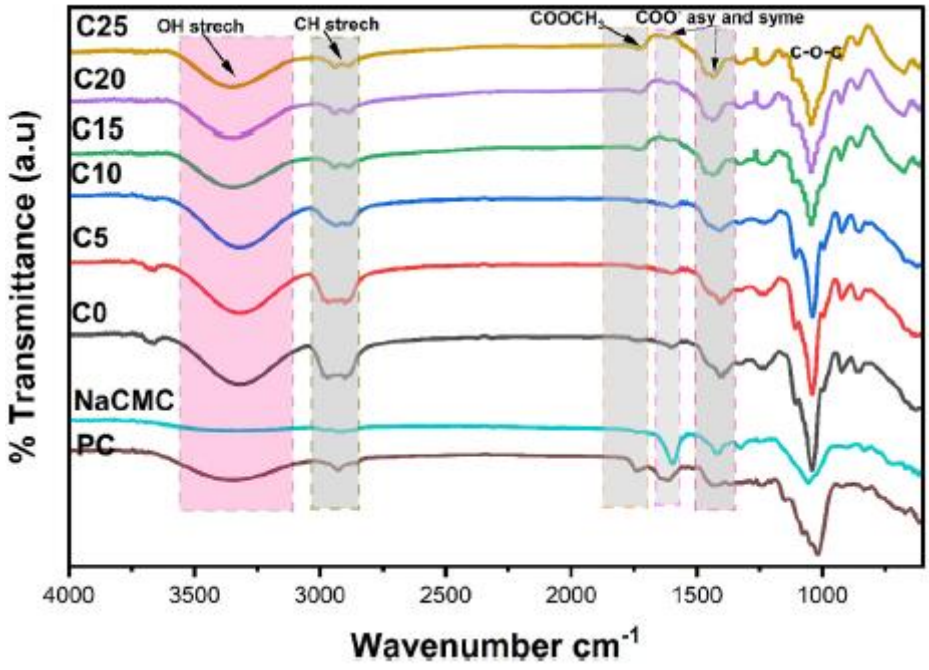

Fig. 1. FTIR spectra of pure PC, pure $NaCMC$ and plasticized $NaCMC/PC$-NH_4Br biopolymer electrolytes.

2.3.4. Scanning electron microscope

The surface morphology was analyzed using a Phenom Pro desktop scanning electron microscope (SEM) with an accelerating voltage of 5 kV. To minimize the charging effect and potential thermal damage, the prepared samples were coated with a thin layer of Pt using a Quorum Q300 TT sputter coater, and SEM characterization was performed at magnification of 1000×.

2.3.5. Thermogravimetric analysis

The thermal stability of the plasticized biopolymer electrolyte samples was evaluated using a thermogravimetric analyzer (TA Q500). The measurements were conducted under a nitrogen gas

atmosphere at a flow rate of 100 mL min^{-1}. Samples weighing approximately 5-8 mg were heated from room temperature to 1000 °C at a rate of 10 °C min^{-1}.

2.3.6. Differential scanning calorimetry

The glass transition temperature (T_g) of the plasticized biopolymer electrolytes were examined using differential scanning calorimetry (DSC).

Table 2 Summary of Functional Groups and Their Corresponding Wavenumbers in $NaCMC/PC$-NH_4Br SPE.

Samples	Functional group and their wavenumber (cm^{-1})					
	C-O-C Stretching	O-H bending	$-COO^-$ Symmetric streaching	$COOCH_3$ Stretching	C-H Stretching	O-H Stretching
C0	1041	1237	1404	1603	2924	3331
C5	1040	1232	1404	1598	2938	3331
C10	1038	1228	1427	1593	2938	3340
C15	1045	1232	1435	1729	2942	3349
C20	1045	1232	1444	1729	2947	3353
C25	1044	1232	1449	1730	2945	3361

2.3.7. Transference number measurement

Transference Number Measurement (TNM) was carried out using the KEITHLEY 6517B Electrometer/High Resistance Meter. A symmetric cell configuration consisting of stainless steel blocking electrodes and an electrolyte layer in between was used. A direct current (DC) voltage of 100 mV was applied to the cell, and the resulting current was continuously monitored over time to determine the transference number.

2.3.8. Linear sweep voltammetry

The electrochemical stability of the SPE was evaluated via linear sweep voltammetry (LSV) using an Autolab PGSTAT-128 N potentiostat. The electrolyte was installed in a Swagelok cell between two stainless-steel electrodes at an applied scan rate of 5 mV s^{-1}.

3. Results and discussion

3.1. Fourier transform infrared ($FTIR$) spectroscopy

The complexation between the salt and the polar groups present within the polymer matrix was determined by analyzing the changes in the $FTIR$ spectra (wavenumbers/intensity). These spectral changes provided clear insights into the interactions occurring within the polymer blends and their interactions with NH4Br. **Fig. 1** shows the $FTIR$ spectra of the pure PC and $NaCMC$. It can be seen from **Fig. 1** that PC shows characteristic bands at 3370 cm^{-1},2927 cm^{-1},1746 cm^{-1},1616 cm^{-1},1428 cm^{-1},1240 cm^{-1} and 1026 cm^{-1}, which correspond to OH, CH, $COOCH_3$, $-COO^-$asymmetric, $COO-$ symmetric, OH bending and glycosidic bond, ring $C-O-C$ respectively [**24**],On the other hand,

$NaCMC$ exhibits absorption bands at 3350 cm^{-1},2900 cm^{-1},1597 cm^{-1},1419 cm^{-1},1325 cm^{-1} and 1058 cm^{-1} which correspond to OH, CH, $COO-$,CH_2, OH bending, and ($C-O-C$), respectively [**25**].

The interactions between MC and the PC polymers were successfully confirmed via the formation of repeating hydrogen bonds between the hydrogen atom of the hydroxyl group (OH) present in the CMC backbone and the oxygen atom existing in the glycoside linkage ($C-O-C$) band of the PC spectra. [**20,23**].

Fig. 1 reveals the presence of six absorption bands for the plasticized -($SPEs$), which exhibited changes in position as the salt concentration varied. These bands include $C-O-C$ stretching, $O—H$ bending, $-COO-$symmetric stretching, -$COOCH_3$ stretching, $C—H$ stretching, and O—H stretching, which correspond to wavenumbers 1041,1237,1404, 1603, 2924, and 3331 cm^{-1}, respectively [**26,27**].

The absorption bands and their corresponding wavenumbers shifted upon addition of different concentrations of wt% of NH_4Br salt are shown in **Table 2**. The $FTIR$ spectrum of the $C0$ sample showed an $O—H$ band at 3331 cm^{-1}. This band is mainly correlated to the formation of hydrogen bonds between the $O—H$ of glycerol and the $O—H$ functional groups of the $NaCMC/PC$ blend, as shown in **Fig. 2**. After the addition of NH4Br, the intensity of the OH peak decreased and shifted towards higher wavelengths.

It can be seen from the $FTIR$ spectra of samples C5 and C25 that the -OH peak occurs at 3331 and 3361 cm^{-1}, respectively. The shift of the $-OH$ peak towards higher wavelengths suggests the complexation between the oxygen atom of the $NaCMC/PC$ blend and NH_4^+ cations via ion coordination bonds [**22**].

The peak observed at 2929 cm^{-1} in the spectrum of the pristine plasticized $NaCMC/PC$ polymer blend corresponds to the $C—H$ stretching vibration. The reduction in the intensity of this $C—H$ peak with the addition of NH_4Br provides vital evidence of complexation between the polymer matrix and the NH4Br salt [**20**]. The vibrational peak at 1746 cm^{-1} is assigned to the $C=O$ stretching vibrations of the polymer blend. Because the major coordination bonds between NH_4^+ cations and polar groups of polymers are considered to occur at the $C—O$ peak, we observed that the peak intensity is suppressed for the biopolymer electrolytes C0, C5, and C10. However, after the addition of salt to biopolymer electrolytes C15, C20, and C25, the intensity of this band broadened and shifted towards higher wavelengths at 1724, 1725, and 1730 cm^{-1}, respectively, suggesting an interaction between the $C=O$ within the polymer blend and NH4Br salt [**28**]. The vibrational peak observed at 1400 cm^{-1} corresponds to the carbonyl group of the carboxylate ion, $COO-$, in the biopolymer electrolyte. It can be seen from the IR spectrum that as the salt concentration increased, the band intensity broadened and shifted towards a higher wavelength. This shift was due to the interaction between the carbonyl group of carboxylate ion and NH_4^+ cations of NH_4Br salt [**28**].

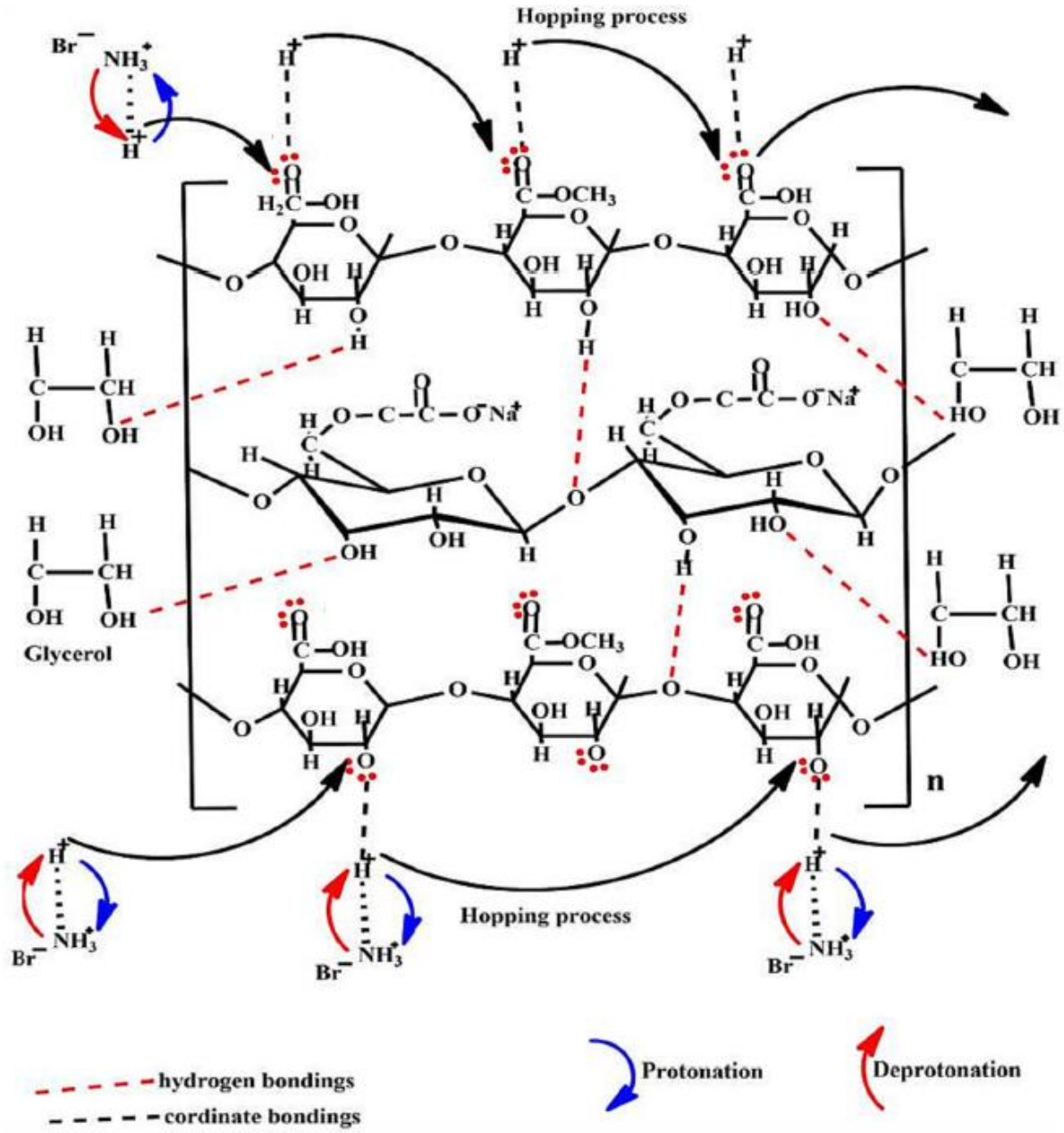

Fig. 2. Proposed interactions between polymer blend $NaCMC/PC$, N_4Br, and glycerol.

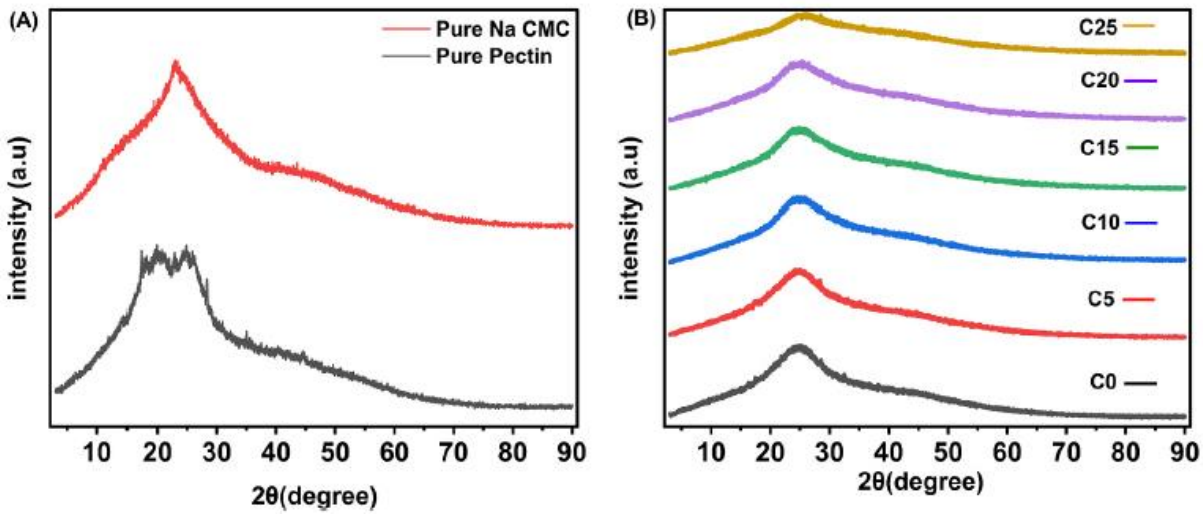

Fig. 3. XRD patterns of pure PC,$NaCMC$ and the plasticized biopolymer blend $NaCMC/PC$ with different concentrations of NH_4Br (wt%).

Table 3 Sample designation and the crystallinity index (x) of plasticized-($SPEs$).

Sample designation	Area under all crystalline peaks A_c	Area under all amorphous peaks A_a	Crystallinity index χ (%)
C0	20,777.91	35,273.67	37.06
C5	18,445.09	33,346.48	35.61
C10	18,035.51	35,706.1	33.55
C15	14,494.73	33,185.31	30.40
C20	6582.18	42,989.83	13.27
C25	4545.57	33,377.93	11.98

3.2. X-ray diffraction analysis

XRD was utilized to investigate the amorphous/crystalline structure change of the prepared plasticized $SPEs$. **Fig. 3** shows the XRD patterns of the pure PC, pure $NaCMC$, and doped plasticized $NaCMC/PC$ $SPEs$. It can be observed from **Fig. 3** (A) that pure $NaCMC$ displays a distinct and broad peak located at a 20 angle of 23°, corresponding to the (200) crystalline plane [**29,30**], while pure PC shows a broad halo peak with few characteristic peaks observed at 20 angles of 18°,20°,22°,24° suggesting its crystalline structure [**31**]. According to $JCPDS$ file no. (85-099), NH_4Br exhibits sharp and intense peaks at 20=30°,38°,44°,49°, and 55°, indicating its crystalline structure [**32**]. As shown in **Fig. 3** (B), all crystalline peaks of NH_4Br disappeared entirely from the XRD pattern of the solid polymer electrolyte, indicating complete dissolution of the salt in the polymer blend matrix. The XRD spectra of the plasticized $SPEs$ exhibited an amorphous peak centered at 20 =24° after the addition of NH_4Br, and the peak became broader and less intense. Hodge et al. [**33**] explained the change in peak amorphousness, where the approach depicted the correlation between crystallinity and peak intensity. The reduction in intensity and broadening of the peaks observed at 20 angles ranging from 3° to 90° indicates that the plasticized $SPEs$ exhibited increased amorphousness following the introduction of salt.

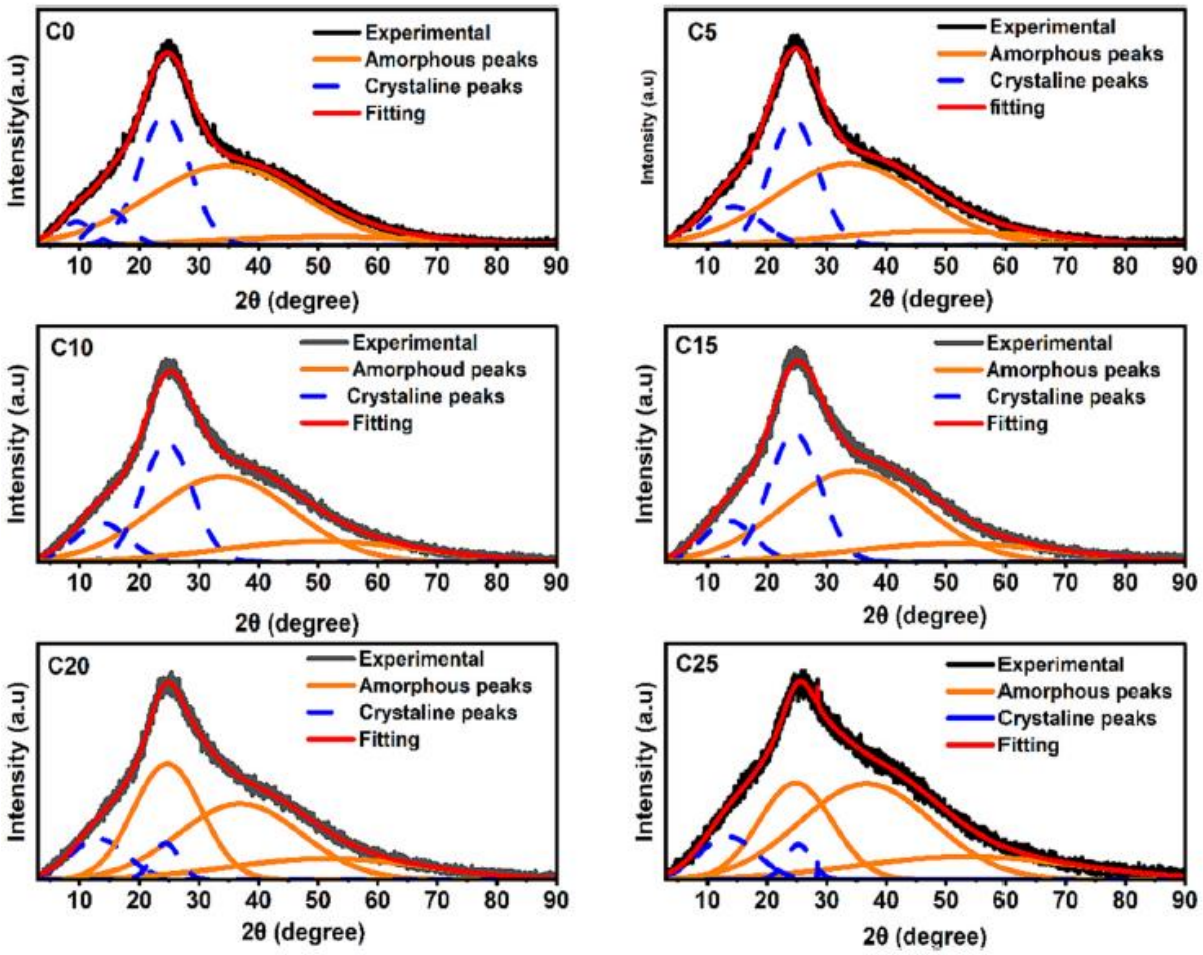

Fig. 4. Deconvoluted XRD patterns of the plasticized biopolymer blend $NaCMC/PC$ with different concentrations of NH_4Br (wt%).

The XRD spectrum is shown in **Fig. 3**(B). was deconvoluted to separate the amorphous and crystalline regions under a broad halo in the XRD diffractogram using free Fityk software. Previous studies demonstrated that cellulose has an amorphous structure and exhibits diffraction peaks located at 20 = 14.64°, 16.05°, and 22.05°, corresponding to the (1 —10), (110), and (200) crystalline planes of $NaCMC$, respectively [**34**]. While pectin is crystalline and has a characteristic peak at 20 = 9.11°, 12.68°, 18.47°,24°, 28.25°, and 40.01° [**31,35,36**] In contrast, the X-ray diffractograms of the biopolymer blend showed a broad peak at 20 = 24°, which could be attributed to the amorphous nature of the plasticized $SPEs$. Hence, the deconvoluted peaks of both polymers were compared to those reported in the literature. Prior to the deconvolution process, a two-point baseline correction method was implemented.

The degree of crystallinity from deconvoluted XRD patterns of plasticized $SPEs$ was evaluated using Eq. (**7**)

$$\chi = \frac{A_c}{A_c + A_a} \times 100\% \qquad (7)$$

where A_c and A_a represent the amorphous and crystalline peak areas, respectively. The degree of crystallinity (x) is listed in **Table 3**.

Fig. 4 illustrates the deconvoluted XRD pattern of the plasticized $SPEs$ system. According to this pattern, a reduction in the intensity of the crystalline peaks associated with the (200) plane is observed. It can be observed from **Table 2** that the addition of (5 wt%) NH_4Br salt caused a reduction in crystallinity from 37.06% to 35.61%. Further increasing the amount of NH_4Br to (25 wt.) % has significantly decreased the degree of crystallinity of plasticized $SPEs$ to 11.98%. These results confirmed the interaction between the characteristic groups of the polymer matrix and NH_4Br salt [**16**].

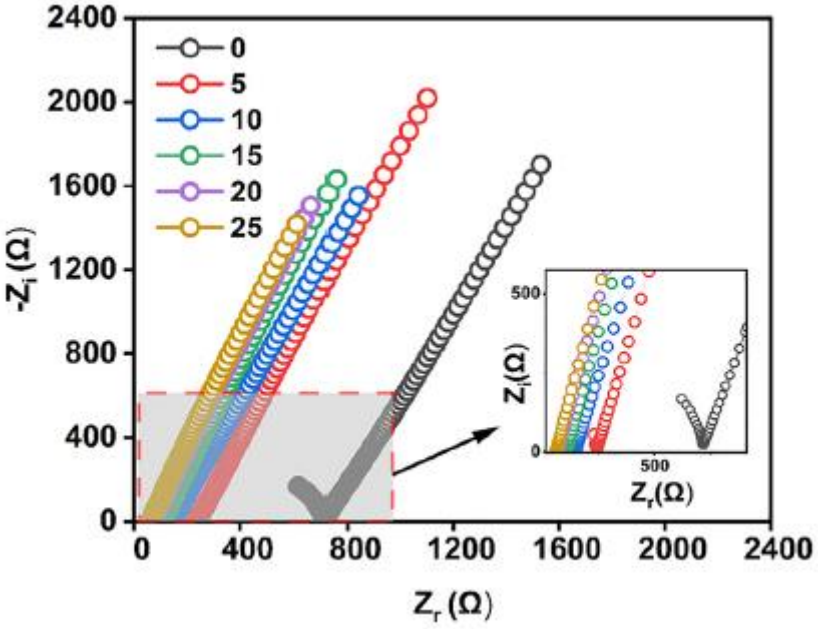

Fig. 5. Nyquist plots for the prepared plasticized biopolymer blend electrolytes doped with different concentrations of NH_4Br (wt%).

Table 4 Bulk resistance (R_b), bulk conductivity σ (S cm^{-1}), DC conductivity (σ_{dc}) and relaxation time (τ) for plasticized $NaCMC/PC$-NH_4Br system.

Sample	R_b (Ω)	σ (S cm^{-1})	σ_{dc}(S cm^{-1})	τ(s)	ω_{max}(Hz)
C0	717	4.07×10^{-5}	7.40×10^{-5}	1.35×10^{-5}	74,074
C5	244	9.01×10^{-5}	8.50×10^{-5}	4.33×10^{-6}	230,946
C10	150	1.99×10^{-4}	1.94×10^{-5}	3.67×10^{-6}	272,479
C15	113.5	2.51×10^{-4}	2.44×10^{-4}	3.12×10^{-6}	320,512
C20	72.2	3.60×10^{-4}	3.45×10^{-4}	2.02×10^{-6}	495,049
C25	60.7	4.68×10^{-4}	4.62×10^{-4}	1.81×10^{-6}	552,486

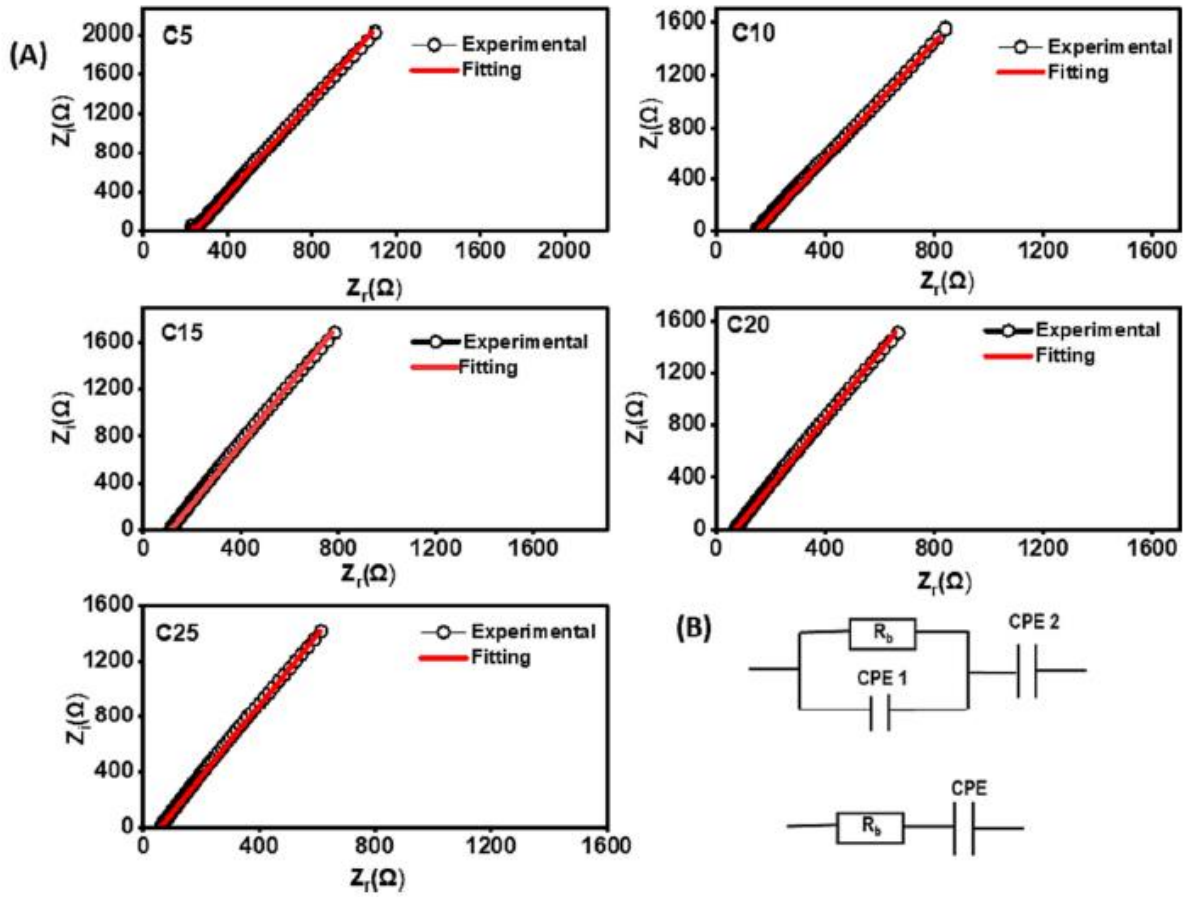

Fig. 6. (A) Nyquist plot with experimental (black circles) data and their fit (red solid line) for plasticized biopolymer blend electrolyte with different concentrations of NH4Br (wt%), (B) Electrical equivalent circuit used for the fit. (For interpretation of the references to colour in this figure legend, the reader is referred to the web version of this article.)

3.3. Electrical impedance spectroscopy

Fig. 5 shows a Nyquist plot representing two major regions: a depressed semicircle in the high-frequency region and an inclined straight line in the low-frequency region. The low-frequency inclined straight line corresponds to electrode polarization due to the accumulation of free charge carriers at the interface between the electrode and electrolyte surface. At the same time, the depressed semicircle on the high-frequency side represents ion/electron conduction in the bulk electrolyte [37]. The depressed semicircle shifted to the high-frequency region, indicating decreased bulk electrolyte resistance. It can be seen from the plot that the semicircular arc at high frequencies vanishes for the C10, C15, C20, and C25 samples, suggesting an increase in ionic conductivity (see **Table 4**), which can be attributed to the increased ionic mobility and higher concentration of ions within the $BPEs$. Moreover, this can be linked to the increasing amorphous phase of the plasticized $SPEs$, as confirmed by the analysis of the XRD spectra [**38**].

In the Nyquist plots of C0 and C5, the R_b value was determined by identifying the point of intersection between the low-frequency side semicircular arc and the high-frequency side- slanted spike. In the Nyquist plot of C10-C25, the Rb value was obtained at the intersection of the spike and the real impedance axis. EIS spectrum analysis software was employed to determine the electrical equivalent circuit (EEC). The solid red line corresponds to the EEC model, which fits the experimental data well **Fig. 6** (A).

The EEC for the C5 sample shown in **Fig. 6** (B) consists of a parallel combination of a constant phase element (CPE1) and resistance (R_b), connected in series with another constant phase element (CPE2). These constant phase elements essentially function as leaky capacitors. The resistance component R_b, within the EEC signifies resistance to the flow of ions or electrons in the sample when subjected to an alternating current field. The Nyquist plot for the C10-C25 samples was analyzed using a circuit model, which included a resistor connected in series with a constant phase element (CPE). This model was chosen because the Nyquist plot displays a distinct tilted spike shape [**16**].

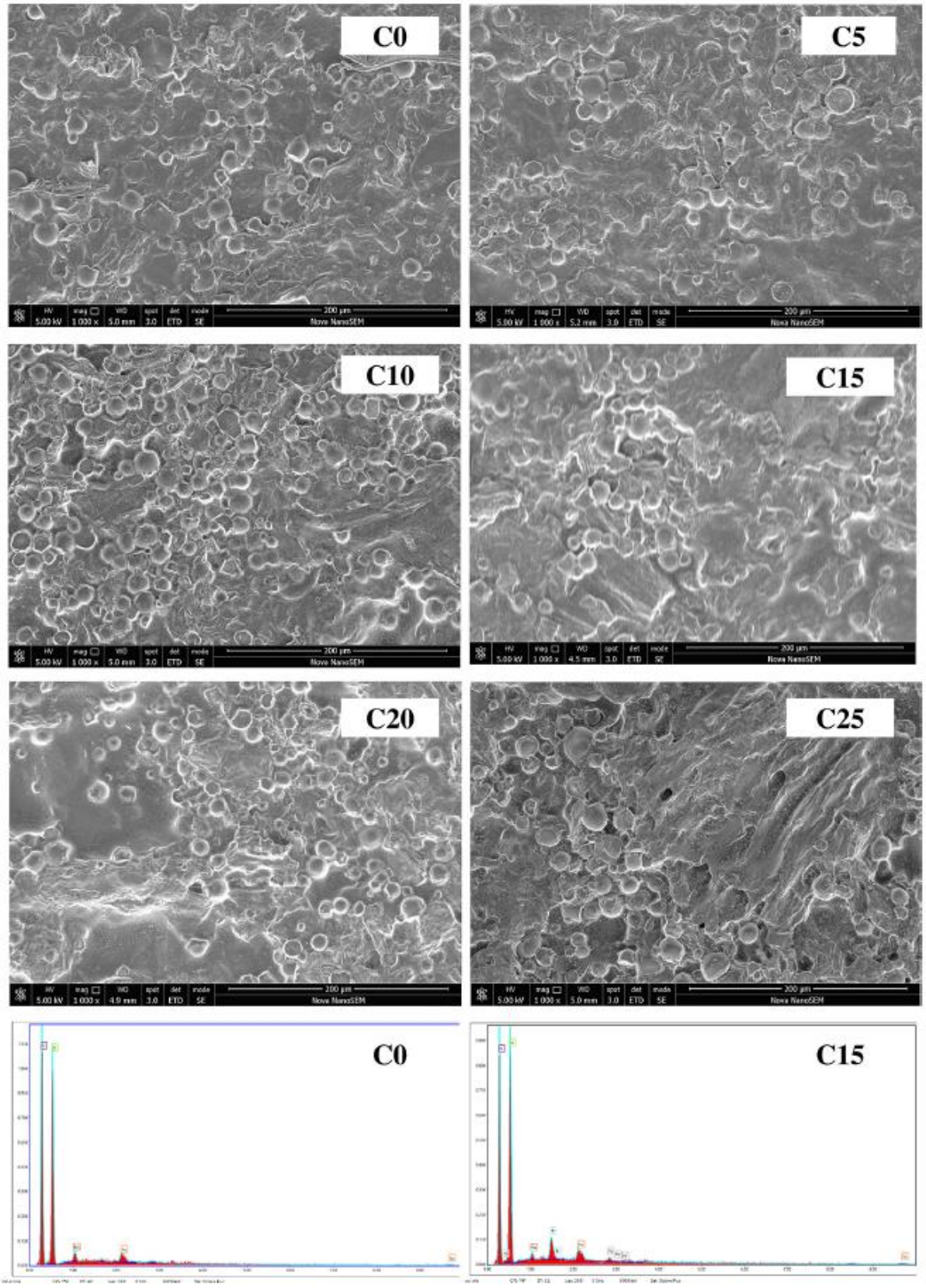

Fig. 7. SEM images of C0-C25 samples along with $EDAX$ spectra of C0 and C15 samples.

3.4. Scanning electron microscopy (SEM)

Fig. 7 shows the SEM micrograph of the samples at a magnification of 1 kX. All samples show a morphology consisting of micro pores with uneven lamellar and rough surfaces without any phase separation. The presence of micro pores in all the samples might be due to the rapid evaporation of the solvent due to the interconnection networks of polymers generated by plasticizers[**39**]. The absence of phase separation indicates the affinity of $NaCMC - PC$ as a blend component [**40**]. The increase in salt concentration resulted in a significant change in the porous structure. The pores merged to form a more distributed, wavy, amorphous lump between the samples (C15-C25). The appearance of pores, along with the existence of a wavy surface with the entrapment of the plasticizer, may be due to the formation of new pathways for ions that can facilitate an increase in ionic conductivity [**41**]. These changes in morphology are due to the interaction of the dissociated ions with the polymer host, as indicated by $FTIR$ studies [**42**]. The $EDAX$ spectrum of C0 shows the presence of all the important elements, such as C, O, and Na. In contrast, the C15 sample showed the presence of all these elements along with Br, indicating that the doping process of NH_4Br into the plasticized polymer system was successful.

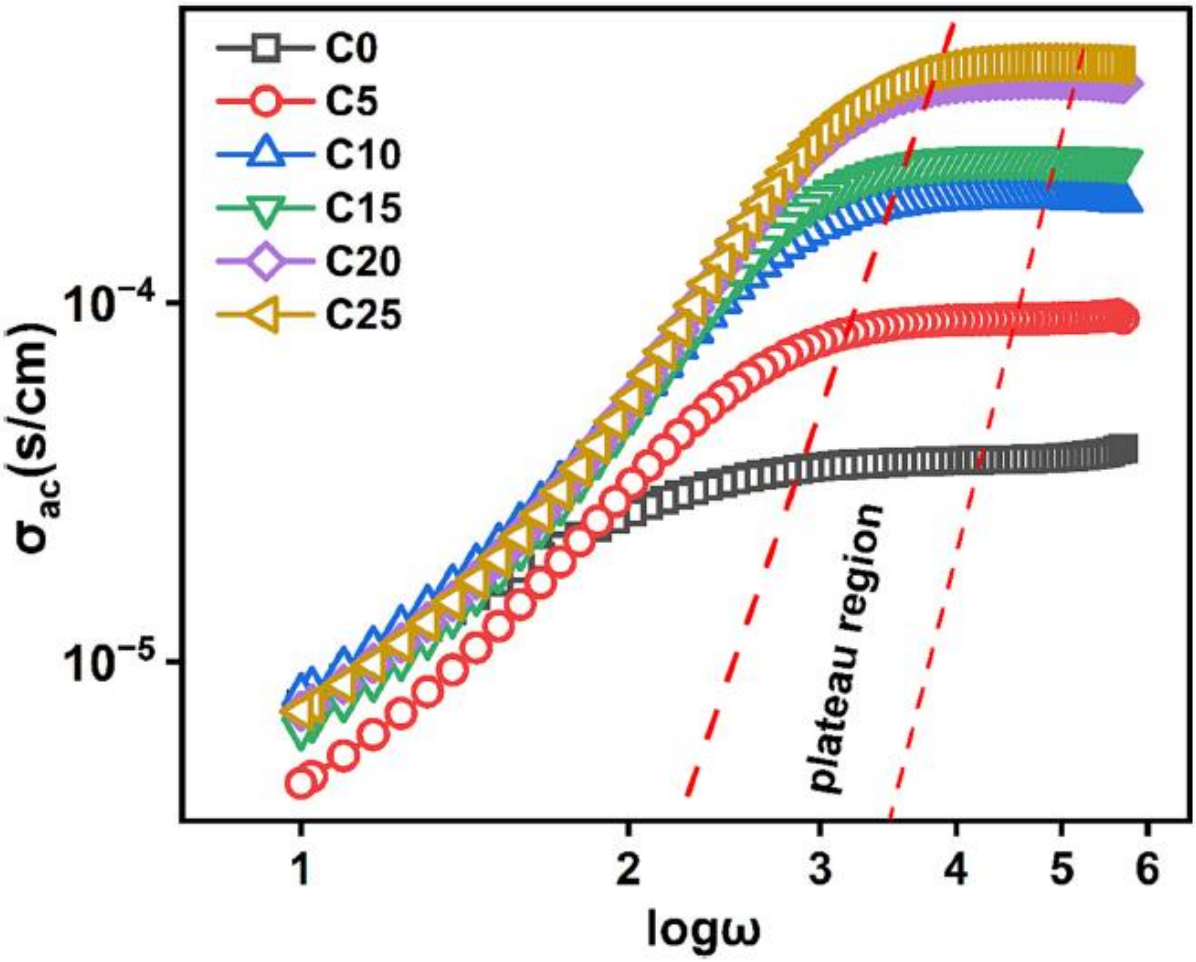

Fig. 8. AC conductivity spectra of the plasticized biopolymer electrolyte incorporated with NH_4Br salt.

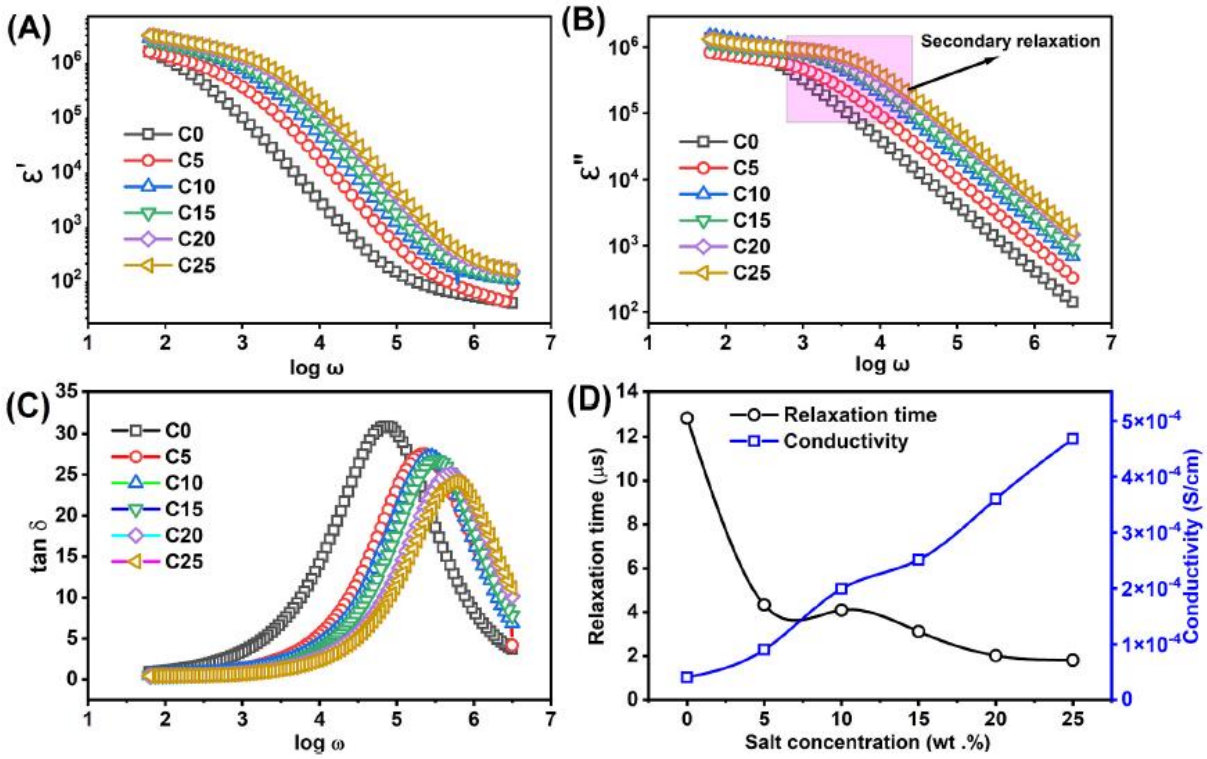

Fig. 9. Frequency dependence of (A) ε' , (B) e and (C) tan S for the plasticized biopolymer blend electrolyte $NaCMC/PC$ doped with NH_4Br salt.

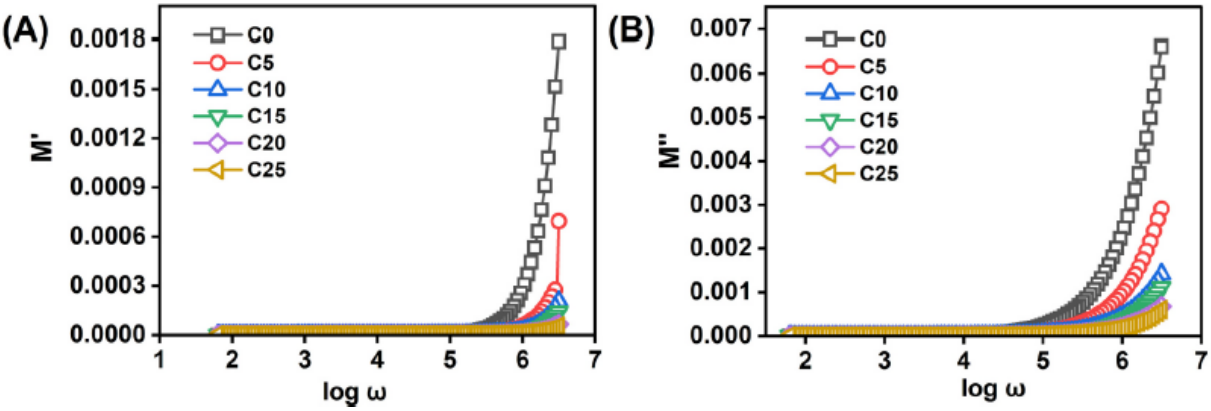

Fig. 10. Plot of (A) M' and (B) M'' dependence on frequency for the prepared plasticized blend electrolytes.

3.5. AC conductivity studies

Fig. 8 illustrates the correlation between adc and loga. The adc values were determined via Eq. (**8**) [**38**].

$$\sigma_{dc} = \left[\frac{Z_r}{Z_r^2 + Z_i^2}\right] \times \left(\frac{t}{A}\right) \qquad (8)$$

The plot can be divided into two distinct sections. In the first section, the dispersion region corresponds to lower frequencies. In this region, the conductivity decreased owing to the accumulation of ions at the electrode interface, resulting in a slower response. Simultaneously, the second section of the graph depicts higher frequencies and appears as a horizontal line, suggesting that conductivity is only minimally affected by the increase in frequency. By extrapolating the plateau region onto the adc axis,

the behaviour of the DC conductivity is shown in Table 4. The DC conductivity estimated in **Fig. 8** aligns with the findings in **Fig. 5**, thereby confirming the conductivity values of the plasticized $NaCMC/PC$-NH_4Br polymer electrolyte [**43**].

3.6. Dielectric study

Dielectric studies play a crucial role in gaining insight into the conductivity and relaxation mechanisms of solid polymer electrolytes ($SPEs$). These studies employed complex permittivity as a fundamental tool for expressing and understanding this phenomenon. The complex permittivity ε^* can be expressed as $\varepsilon^* = \varepsilon' - j\varepsilon''$, where ε′ represents the real part associated with the polymer's ion dissociation capacity, whereas ε′represents the imaginary part related to the energy needed for dipole alignment and ion movement [**44**]. The variations in these three parameters as a function of frequency are shown in **Fig. 9** (A).

At lower frequencies, both e and e displayed high values, which is primarily attributed to the electrode polarization. This phenomenon occurs as ions accumulate at the interface between the electrode and electrolyte, resulting in a substantial increase in the dielectric constant value After that, the dielectric constant exhibits a non-linear decrease as frequency increases until it reaches a constant value. This nonlinear decrement is correlated with the difficulty that ions find following the field at higher frequencies [**44**]. **Fig. 9** (B) illustrates a y relaxation peak observed in the mid-frequency range, which is known as secondary relaxation and occurs below the glass transition temperature (T_g). Secondary relaxations are generally categorized as β, γ and σ relaxations. β relaxation involves the movement of the monomer unit of $NaCMC$ through a glycosidic bond, while the y relaxation is associated with the motion of side chains in the $NaCMC$ unit. The σ relaxation corresponds to ion migration or hopping at high temperatures [**45**].

As shown in **Fig. 9** (B), the relative intensity of the γ peak increased and shifted towards higher frequencies. This phenomenon is accompanied by an increase in conductivity, which can be associated with the γ-relaxation peak of NaCMC with the side chain motion of $Na - CMC$ via OCH_2COONa [**46**]. **Fig. 9** (C) depicts the variation in the tangent loss,$tan\delta$, as a function of the frequency. This peak corresponds to conductivity relaxation, which differs from the γ relaxation. At lower frequencies, an increase in $tan\delta$ with frequency occurs because of the higher dominance of the active component (ohmic) compared to the reactive component (capacitive). On the other hand, at higher frequencies $tan\delta$ decreases with frequency because the ohmic portion is independent of frequency, and the reactive component grows proportionally with the frequency [**47**]. The relaxation time is calculated using Eq. (**9**)

$$\omega_{max}\tau = 1 \qquad (9)$$

As the salt concentration increased, the maximum peak of tanS shifted towards higher frequencies. This shift signifies a reduction in the relaxation time (see **Table 3**), which is commonly associated with the polymer chain flexibility that facilitates the movement of ions via the coordinating sites, assisted by the segmental motion of the polymer chain [**48**].

Fig. 9 (D) illustrates the relationship between relaxation time and DC conductivity. Upon addition of salt, the DC conductivity increased and reached a maximum at (25 wt%). Simultaneously, the relaxation time decreased and reached a minimum value at the same salt concentration. This indicates

that the incorporation of more salt enlarges the amorphous phase, leading to an increased orientation of the polymer chains and ultimately resulting in a reduction in the relaxation time [**48**].

3.7. Modulus spectrum analysis

The dielectric modulus tool has been extensively used to investigate the conductivity relaxation processes in solid polymer electrolytes. At lower frequencies, as is evident from **Fig. 10**, both the real and imaginary components of the dielectric modulus exhibit a long tail converging towards zero, supporting the capacitive nature of the SPE. This behaviour is due to the minimal impact of electrode polarization within this frequency range. Moreover, the graph shows both an increase in M values and a shift of the peak towards higher frequencies up to the C25 sample. The same trend can be seen in M plot. This phenomenon can be associated with the occurrence of ion-hopping and relaxation mechanisms facilitated by structural flexibility [**49**].

3.8. Ion transport properties

The Nyquist plot was used to fit and determine parameters such as the charge carrier density (n), mobility (μ), and diffusion coefficient (D). The plot of C5 displays both a semicircle and a tilted spike. Based on the equivalent circuit model proposed by Arof et al. (2014) [**50**], the graph in **Fig. 6** can be effectively represented by a parallel combination of a constant phase element (CPE2) and a resistor (R_b), which are connected in series with another constant phase element (CPE1). For such an equivalent model, the real part (Z_r) and imaginary part (Z_i) of impedance are defined by Eqs. (**10**) **and** (**11**) respectively.

Table 5 Variation in ion transport parameters with salt concentra

Sample	k_2^{-1} (F)	D (cm^2 s^{-1})	μ (cm^2 V^{-1} s^{-2})	n cm^{-3}	σ (S cm^{-1})
C5	2.04×10^{-5}	1.05×10^{-7}	4.07×10^{-6}	1.37×10^{20}	9.01×10^{-5}
C10	2.94×10^{-5}	2.27×10^{-7}	8.79×10^{-6}	1.41×10^{20}	1.99×10^{-4}
C15	2.53×10^{-5}	2.39×10^{-7}	9.25×10^{-6}	1.69×10^{20}	2.51×10^{-4}
C20	2.90×10^{-5}	3.37×10^{-7}	13.1×10^{-6}	1.72×10^{20}	3.60×10^{-4}
C25	3.09×10^{-5}	3.98×10^{-7}	15.4×10^{-6}	1.90×10^{20}	4.68×10^{-4}

$$Z_r = \frac{R + R^2 k_1^{-1} \omega^{p_1} cos\left(\frac{\pi p_1}{2}\right)}{1 + 2Rk_1^{-1}\omega^{p_1} cos\left(\frac{\pi p_1}{2}\right) + R^2 k_1^{-2}\omega^{2p_1}} + \frac{cos\left(\frac{\pi p_2}{2}\right)}{k_2^{-1}\omega^{p_2}} \tag{10}$$

$$Z_i = \frac{R^2 k_1^{-1} \omega^{p_1} sin\left(\frac{\pi p_1}{2}\right)}{1 + 2Rk_1^{-1}\omega^{p_1} cos\left(\frac{\pi p_1}{2}\right) + R^2 k_1^{-2}\omega^{2p_1}} + \frac{sin\left(\frac{\pi p_2}{2}\right)}{k_2^{-1}\omega^{p_2}} \tag{11}$$

where ω is the angular frequency, R is the bulk resistance, k_1^{-1} is the bulk capacitance arising from the polar group in bulk k_2^{-1} is the double layer capacitance due to accumulation of the ions, the parameter p_1 corresponds to the ratio of the angle formed between the diameter of the semicircle and the vertical axis, to the right angle formed by the real and imaginary impedance axes. The symbol p_2 represents the skew parameter, which regulates the extent to which the main spike deviates from the real axis. The values of p_1 and p_2 lie between 0 and 1.

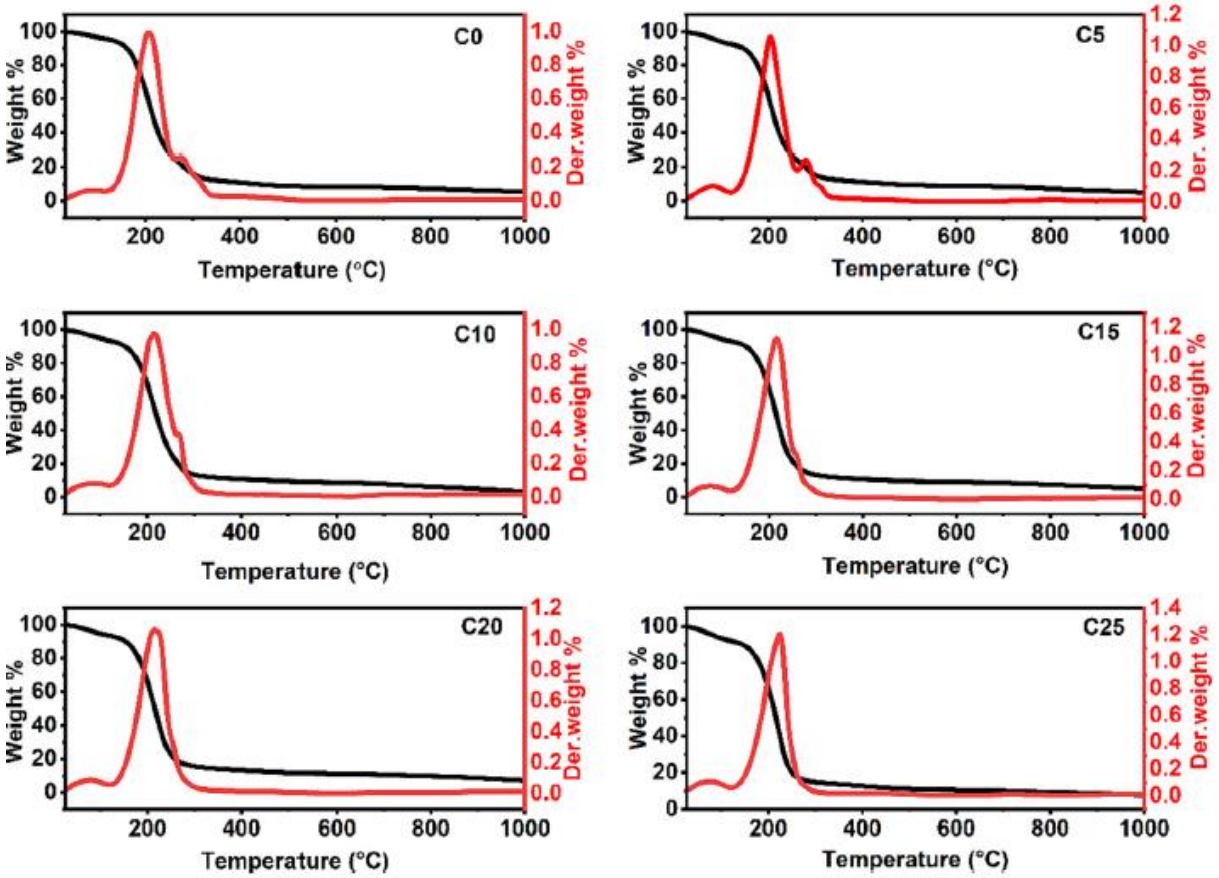

Fig. 11. The variation in the transport parameters as a function of NH_4Br(wt%) for plasticized-($SPEs$).

In the case of the second type of Nyquist plot, the equivalent model can be depicted as a resistor connected in series with a constant phase element (CPE1). For this type of equivalent model, the Z_r and Z_i can be described using Eq. (**12**) **and** (**13**) respectively:

$$Z_r = R + \frac{cos\left(\frac{\pi p}{2}\right)}{k^{-1}\omega^p} \tag{12}$$

$$Z_i = \frac{sin\left(\frac{\pi p}{2}\right)}{k^{-1}\omega^p} \tag{13}$$

Here R is the bulk resistance while k^{-1} and p represent the same values mentioned above in Eqs. (**10**) **and** (**11**) The calculation of charge transport parameters, such as the diffusion coefficient (D), mobility (μ) and number density (n) of charge carriers, involved the utilization of the following Eqs. (**14**) **to** (**16**).

$$D = \frac{e(k_2 \varepsilon_r \varepsilon_0 A)^2}{\tau_2} \quad (14)$$

$$\mu = \frac{eD}{k_B T} \quad (15)$$

$$n = \frac{\sigma}{\mu e} \quad (16)$$

In the given context, ε_t represents the dielectric constant observed at high frequencies, k_b denotes Boltzmann constant (1.38× 10^{-23} Jk^{-1}), T signifies the absolute temperature and the value of τ_2 is chosen at the frequency when Z_i →0.

Table 5 presents the values of n, μ, and D for the plasticized biopolymer electrolytes $NaCMC/PC$-NH_4Br.The addition of glycerol as a plasticizer into the polymer blend system plays a significant role due to the presence of large numbers of OH groups in its chemical structure, which serve as an additional coordinating site for ions. As shown in **Table 5**, the NH_4Br salt concentration, wt% increases, the number of charge carrier's follow the same trend. This observed increment in number density of charge carriers is primarily linked to the dissociation of NH_4Br salt into free NH_4^+ and Br^- ions.

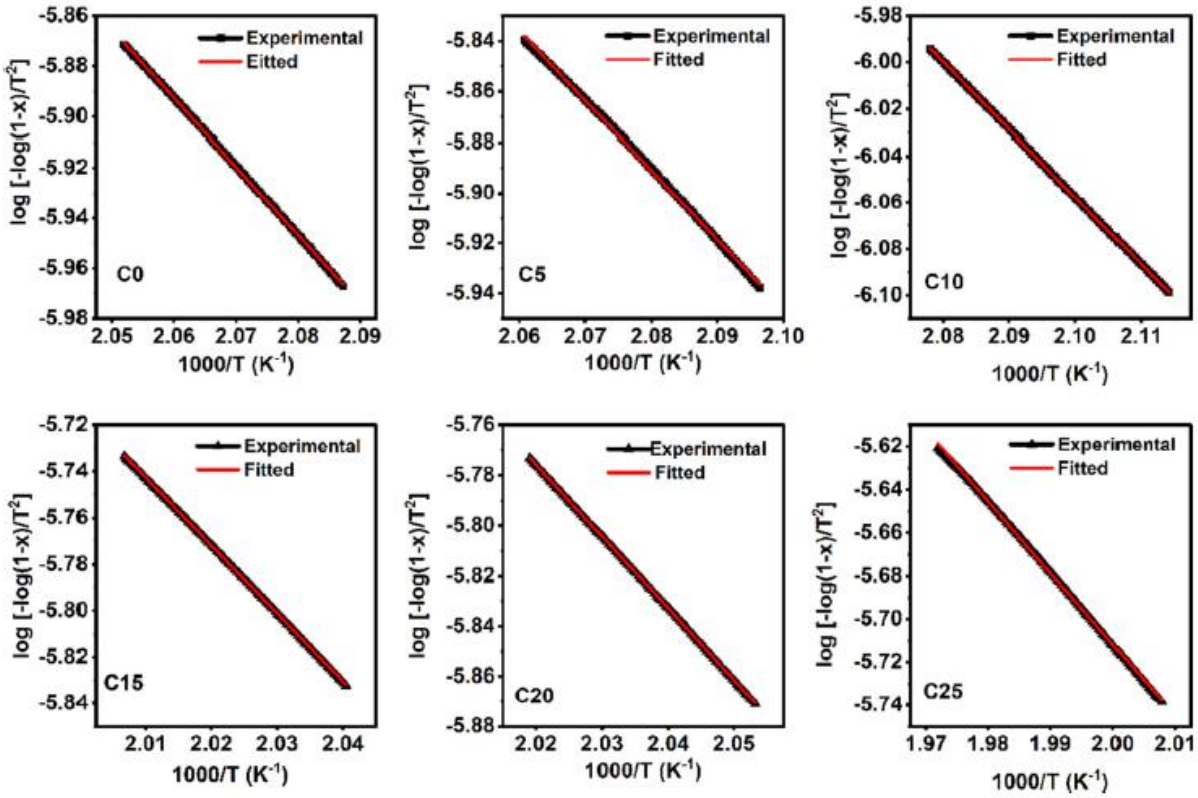

Fig. 12. TGA thermograms of the prepared plasticized biopolymer blend electrolytes.

Table 6 Thermal parameters of prepared plasticized $NaCMC/PC$-NH_4Br electrolytes.

Sample designation	Maximum decomposition temperature T_d (°C)	Maximum decomposition weight loss (%)	Thermal decomposition activation energy Ea (kJ/mol)
C0	205	83.10	51.86
C5	203	79.95	52.62
C10	215	79.50	55.30
C15	216	78.84	56.07
C20	215	77.49	54.54
C25	244	76.40	72.19

This phenomenon leads to the ion-dipole interaction between NH+cations and oxygen atoms present in the $-OH$, $COO-$, and $COOCH_3$ groups of the polymer blend as confirmed by $FTIR$ studies [**51**]. Furthermore, it is evident that the bulk conductivity adc follows the same trend of charge carrier concentration, suggesting that the concentration of charge carriers significantly impacts the increase in ionic conductivity rather than mobility and diffusion coefficient [**45**]. The variation of transport parameters n, μ, and D with different concentration of NH_4Br for plasticized biopolymer electrolytes are presented in Fig. **11**.

3.9. Thermogravimetric analysis

The thermal stability of the polymer electrolyte was evaluated using thermogravimetric analysis (TGA), as illustrated in **Fig. 12**. Two primary steps characterize the degradation process. In the first step, a minor weight loss of (approximately 5%) is observed within the temperature range of 27-130 °C associated with the dehydration process, which involves the removal of trapped liquid and moisture from the polymer electrolyte matrix [**52,53**].The second step, occurring between 130 °C and 300 °C, includes a significant decomposition (approximately 76%), which can be attributed to the cleavage of the saccharide rings, which leads to the depolymerization of pectin chains present in the SPE system [**54,55**]. The weight loss observed during this stage is considerably higher than that observed during the dehydration process. It can be seen from **Table 6** that upon increasing the salt concentration (up to 25 wt%), the decomposition temperature appears to shift towards higher values, which refers to the strong complexation between the salt cation (NH_4^+) and polar groups of the plasticized $NaCMC/PC$ blend. This variation clearly indicates an enhancement in the thermal stability temperature. [**56,57**].

3.10. Calculation of activation energy of thermal decomposition

The activation energy (E_a) associated with the major thermal degradation of polymer electrolytes is determined by employing the integral Eq. (**17**) established by Coats and Redfern [**58**], which is presented as follows:

$$log\left[-\frac{log(1-\alpha)}{T^2}\right] = log\frac{R}{E_a}\left[1-\frac{2RT}{E_a}\right]-\frac{E_a}{2.303RT} \text{ for n} \neq 1 \qquad (17)$$

where E represents the activation, energy defined as the minimum energy required to initiate a phase change in polymer molecules, n is the order of the reaction, T is the temperature in Kelvin, R is the universal gas constant, a is the a fractional parameter at a particular temperature given by Eq. (**18**)

$$\alpha = \frac{w_i - w_T}{w_i - w_f} \tag{18}$$

where wiis the initial weight of the sample, w_T is the weight at a particular temperature T and w_f is the final temperature. For $n = 1$ the Eq. (**17**) takes a new form and becomes

$$log\left[-\frac{log(1-\alpha)}{T^2}\right] = log\frac{R}{E_a}\left[1-\frac{2RT}{E_a}\right] - \frac{E_a}{2.303RT} \tag{19}$$

A linear graph for $\frac{1000}{T}$ vs log $-$ log$\left[-\frac{\log(1-\alpha)}{T^2}\right]$ is shown in **Fig. 13**. The activation energy E_a is determined by calculating the slope of the graph and applying the relation $E = 2303\text{R} \times$ slope. The calculated activation energies (kJ/mol) are presented in **Table 6**. The table shows that the addition of salts results in an increase in the activation energy. This suggests that NH4Br has an impact on the thermal degradation of the plasticized polymer electrolyte, thereby contributing to an improvement in its thermal stability [**59,60**].

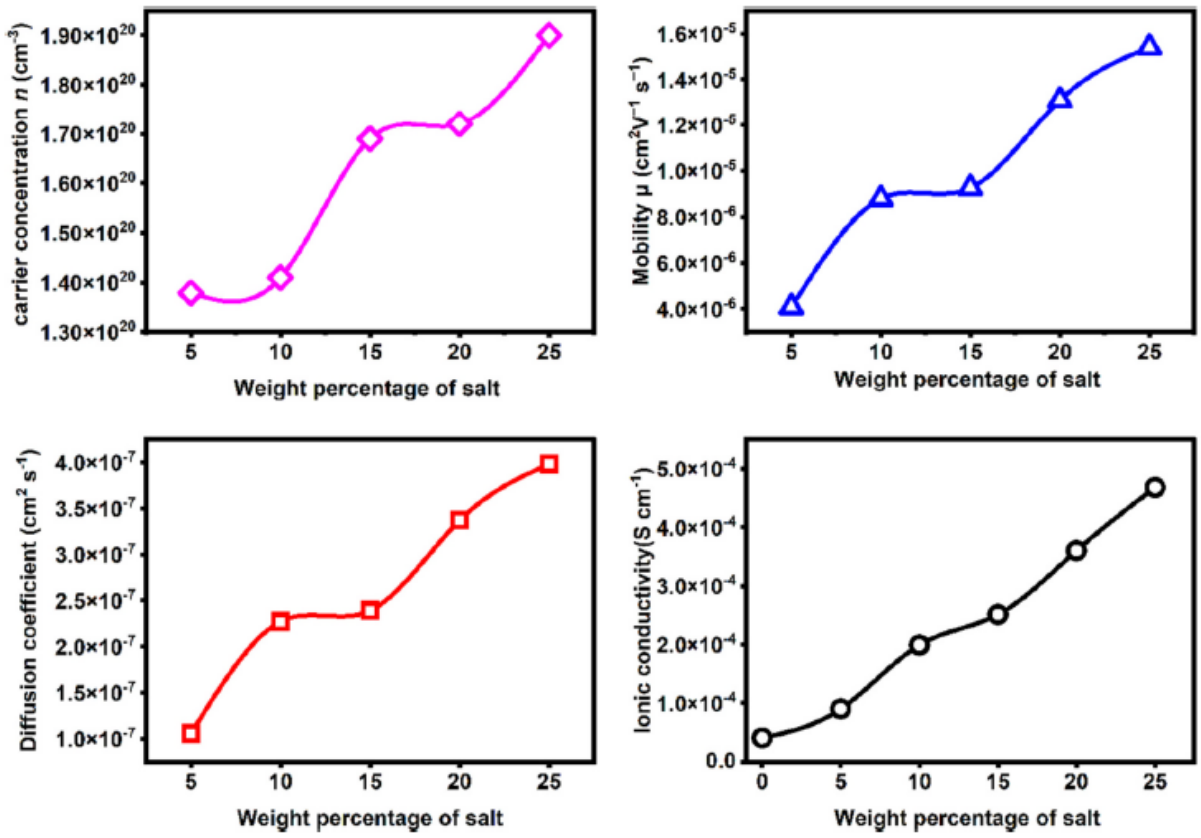

Fig. 13. Plot of log$\left[-\frac{\log(1-\alpha)}{T^2}\right]$ VS $\frac{1000}{T}$ for the plasticized biopolymer electrolytes.

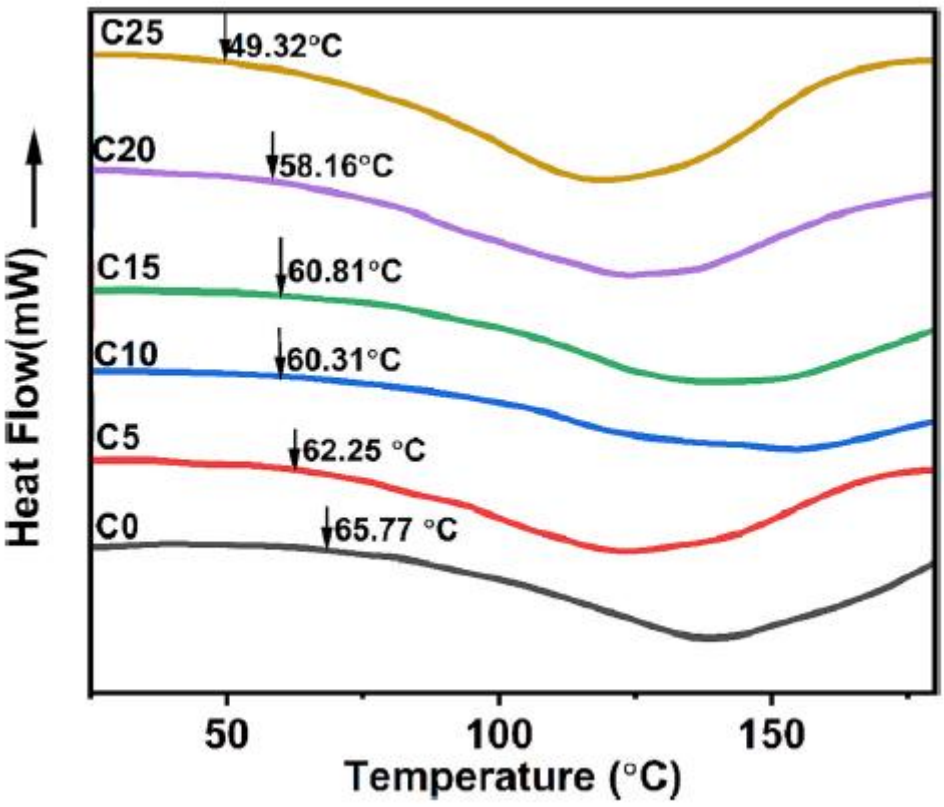

Fig. 14. DSC plots for the prepared plasticized biopolymer electrolytes.

3.11. Differential scanning calorimetry

Fig. 14 shows the DSC thermogram of samples with different wt% concentrations of NH_4Br salt. Each curve demonstrates a single-step transition of an endothermic process, supporting the miscibility of the polymer blend. According to the results published by Dennis et al. [**23**], the T_g of the polymer blend comprising PC and MC was around 99 °C, whereas in the present work, it is observed to be around 66 °C. The decrease in Tg can be attributed to the formation of hydrogen bonds between $NaCMC/PC$ and glycerol. [**26,61**]. After the addition of different concentrations of NH_4Br salt into the polymer blend, T_g for all the samples decreased. This trend can be attributed to the plasticizing effect of NH4Br on the polymer structure [**62**]. The presence of salt plays a crucial role in weakening the dipole-dipole interactions between the $NaCMC/PC$ blend chains, which increases the flexibility of the polymer chains and facilitates the hopping of ions within the polymer backbone, thus increasing the ionic conductivity of the plasticized biopolymer electrolytes. [**28,63,64**].

3.12. Transference number measurements (TNM)

To achieve optimal performance in energy-storage devices, the primary charge carriers must be ions. Moreover, their contribution to the overall electrical conductivity tends to one. The Wagner polarization method was employed to determine the transference numbers for ions (t_{ion}) and electrons (t_{elec}). This technique fundamentally depends on the measurement of the current (I) vs. time (t) [**65**]. The current was measured by applying a constant (DC) voltage of 100 mV to the cell. During DC biasing, the free ions migrate towards electrodes with opposite charges, resulting in the gradual polarization of the cell until it reaches a fully polarized state. Subsequently, an electronic

current flow across the circuit. This suggests that both ions and electrons are responsible for the initial current. However, only electrons contribute to the final current as ions are entirely blocked at the electrodes once the cell is fully polarized [**66**].(**Fig. 15**) illustrates the $I-t$ plot for the plasticized SPE samples.

The determination of ionic and electronic transference numbers involves the utilization of Eqs. (**20**) and (**21**), respectively.

$$t_{ion} = 1 - \frac{I_f}{I_i} \tag{20}$$

$$t_{elec} = 1 - t_{ion} \tag{21}$$

where I_i and I_f represent the initial and final current of the SPE samples, respectively. **Table 7** presents the TNM values for the plasticized $SPEs$, where the total ionic transfer number ranges from 0.89 to 0.96, indicating that ions predominantly contributed to charge transport rather than electrons. Utilizing Eqs. (**22**) and (23, the ionic (σ_{ionic}) and electronic($\sigma_{\text{electronic}}$) conductivity can be determined.

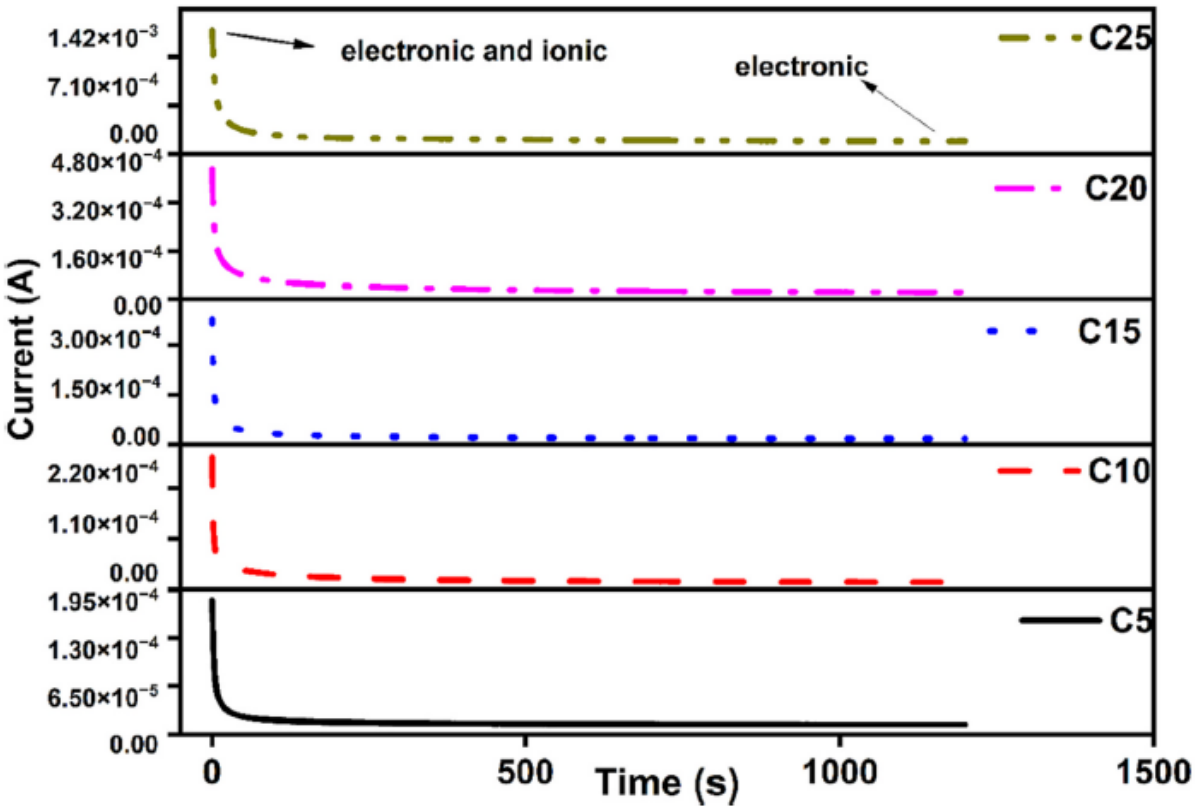

Fig. 15. Ion transport number for plasticized biopolymer electrolytes.

Table 7. Transference numbers values.

Sample designation	t_{ion}	t_{elec}	σ_{ionic} S cm^{-1}	$\sigma_{electronic}$ S cm^{-1}
C5	0.93	0.06	8.37×10^{-4}	5.40×10^{-5}
C10	0.95	0.05	1.89×10^{-4}	9.95×10^{-6}
C15	0.96	0.04	2.40×10^{-4}	1.00×10^{-5}
C20	0.95	0.04	3.42×10^{-4}	1.44×10^{-5}
C25	0.90	0.1	4.21×10^{-4}	4.68×10^{-5}

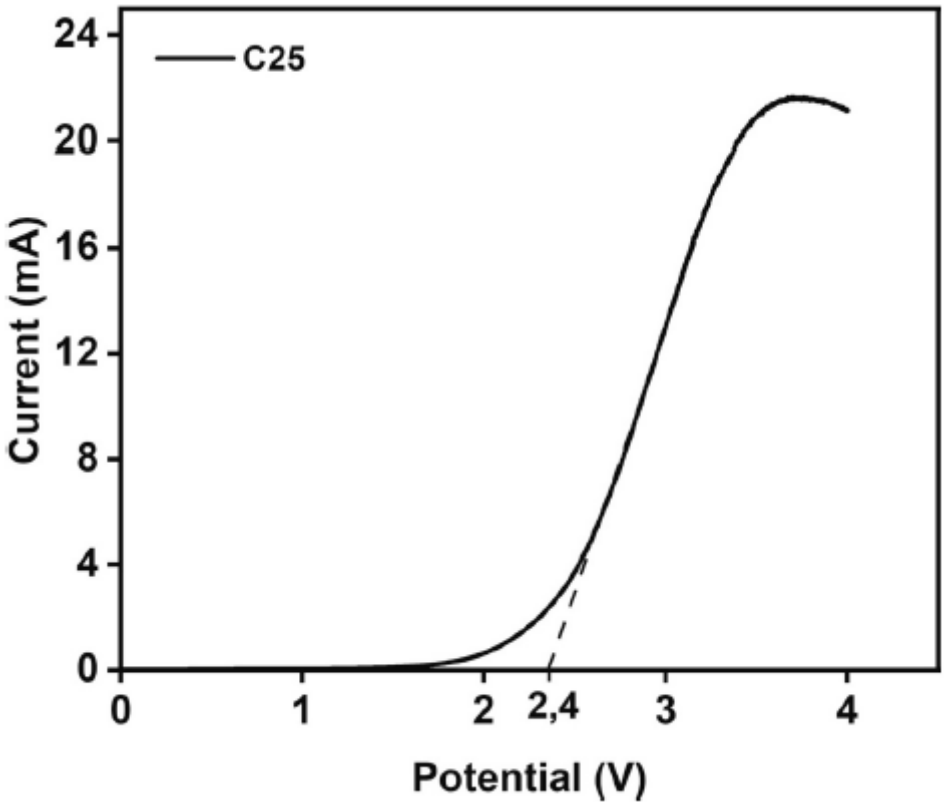

Fig. 16. LSV curve of sample C25.

$$\sigma_{ionic} = t_{ion} \times \sigma \tag{22}$$

$$\sigma_{electronic} = t_{elec} \times \sigma \tag{23}$$

The results illustrated in **Table 7** provide clear evidence that the ionic conductivity is higher than the electronic conductivity, indicating that the prepared plasticized $SPEs$ have promising potential for energy-storage applications.

3.13. Linear sweep voltammetry (LSV)

The electrochemical stability of the plasticized SPE with the highest NH4Br content (25 wt%) salt was evaluated using a potential window 0-4 V and a current rate of 5 mV s^{-1} using LSV (See **Fig. 16**). At potential lower than 2.4 V the current is near 0; however, increasing the potential above that limit, we observed an exponential increase in the current due to the oxidation process at the inert electrode surface. Thus, the maximum voltage limit was determined at a potential of approximately 2.4 V. Below this limit, electrochemical reactions do not occur, and consequently, the SPE can be used in energy devices such as supercapacitors and batteries. Our results show a superior potential window compared with other studies which involved ammonium salt-based electrolytes, such as NH_4Cl with a voltage window up to 1.4 V [**67**], and NH_4NO_3 [**68**] with electrochemical stability up to 1.7 V.

3.14. Fabrication of the primary battery

The primary battery was constructed using the highest-conducting sample, C25, as the medium for charge transport. The anode was created by blending Zn, $ZnSO_4.7H_2O$, and graphite powder at a weight ratio of 3:1:1 using a laboratory mortar until a fine powder was formed. Similarly, the cathode was prepared by combining PbO_2, V_2O_5, and graphite powder at a weight ratio of 8:2:1:0.5. The resulting fine powder from both the anode and cathode was compressed using a pellet-pressing machine under high pressure to form pellets with a diameter (20 mm).

The variation in OCV as a function of time is shown in **Fig. 17** (A). The initial OCV measurement was 1.32, which gradually decreased to 1.1 V and remained stable for 34 h. This initial decrease is attributed to activation polarization [**69**]. **Fig. 17** (B) shows the cell's discharge under a constant current of 0.2 mA. The initial decrease in the voltage was due to the polarization and internal IR drop. Subsequently, the voltage continuously dropped, and a voltage plateau was not observed, indicating that the current electrodes might not be suitable for the optimum sample under study. Similar observations were reported by Pradeep et al. [**70**]. Perhaps, a more suitable electrode needs to be chosen, which is beyond the scope of this research.

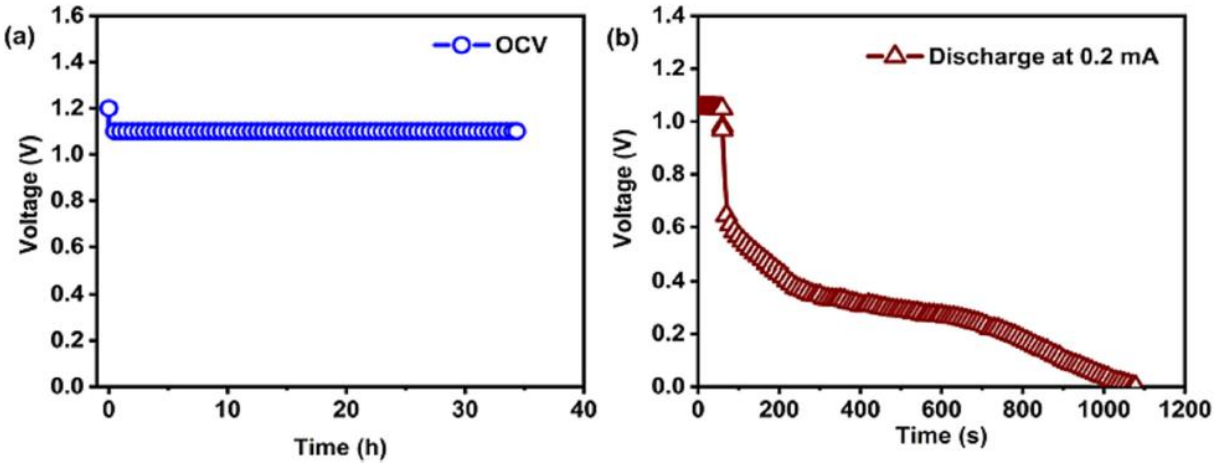

Fig. 17. (A) Open circuit voltage (OCV) of the primary battery, (B) battery discharge under 0.2 mA.

Table 8 Cell parameters.

Parameters	Measured Value with units
Cell diameter (mm)	20
Cell area (cm^2)	3.14
Cell thickness (mm)	2
Cell weight (g)	0.0765
OCV (V)	1.2

Table 9 Comparison of the OCV of the cell with the previous study.

Anode	cathode	OCV (V)	Reference
Zn + ZnSO4	PbO2+ V2O5	0.4	[71]
Zn + ZnSO4	PbO2+ V2O5	1.4	[28]
Zn + ZnSO4	PbO2+ V2O5	1.2	Current work

The cell parameters of the current cell are listed in **Table 8**, and a comparison of the OCV with the previous study is presented in **Table 9**. This indicates the possible application of the optimized sample in electrochemical applications.

4. Conclusion

The solution casting method was used to prepare a novel polymer blend comprising plasticized $NaCMC/PC$ and NH_4Br salts. The structural changes were investigated using X-ray diffraction (XRD) and Fourier transform infrared ($FTIR$) analyses. X-ray diffraction analysis revealed a decreased crystallinity index, which promoted faster ion migration. Furthermore, $FTIR$ studies confirmed the interaction between the salt and plasticized polymer blend, evident through changes in the intensity and shift of the (OH) band at 3348 cm^{-1} towards lower wavelengths. The C25 sample exhibited a high ionic conductivity of 4.68×10^{-4} S cm^{-1}, which is attributed to salt dissociation. DSC analysis indicated a decreased glass transition temperature (T_g), signifying an increased polymer chain flexibility. This finding is consistent with the results obtained from the XRD and impedance analyses, establishing a correlation among these parameters. The incorporation of NH_4Br improved both the overall thermal stability, which remained up to 150 °C (within a safe limit), and the dielectric properties, including the dielectric constant and tangent loss. The transport properties, such as ion mobility (μ), number density (n), and diffusion coefficient (D), were obtained by fitting the Nyquist plots, and were found to be in good agreement with other experimental results. The fabricated battery exhibited an open-circuit voltage (OCV) of 1.2 V. The battery performance can be further enhanced by selecting a suitable electrode.

Appendix A. Supplementary data

Supplementary data to this article can be found online at **https://doi. org/10.1016/j.ssi.2023.116379**.

References

[1] M. Rayung, M.M. Aung, S.C. Azhar, L.C. Abdullah, M.S. Su'ait, A. Ahmad, S.N.A. M. Jamil, Bio-based polymer electrolytes for electrochemical devices: insight into the ionic conductivity performance, Materials. 13 (2020) 838, **https://doi.org/10.3390/ma13040838**.

[2] Y. Wang, W. Zhong, Development of electrolytes towards achieving safe and high-performance energy-storage devices: a review, ChemElectroChem. 2 (2014) 22-36, **https://doi.org/10.1002/celc.201402277**.

[3] H. Wang, Z. Yu, X. Kong, S.C. Kim, D.T. Boyle, J. Qin, Z. Bao, Y. Cui, Liquid electrolyte: the nexus of practical lithium metal batteries, Joule. 6 (2022) 588-616, **https://doi.org/10.1016/j.joule.2021.12.018**.

[4] L. Kong, Y. Li, W. Feng, Strategies to solve lithium battery thermal runaway: from mechanism to modification, Electrochem. Energy Rev. 4 (2021) 633-679, **https:// doi.org/10.1007/s41918-021-00109-3**.

[5] J. Chai, Z. Liu, J. Zhang, J. Sun, Z. Tian, Y. Ji, K. Tang, X. Zhou, G. Cui, A superior polymer electrolyte with rigid cyclic carbonate backbone for rechargeable lithium ion batteries, ACS Appl. Mater. Interfaces 9 (2017) 17897-17905, **https://doi.org/ 10.1021/acsami.7b02844**.

[6] K. Murata, S. Izuchi, Y. Yoshihisa, An overview of the research and development of solid polymer electrolyte batteries, Electrochim. Acta 40 (2000) 1501-1508, **https://doi.org/10.1016/S0013-4686(99)00365-5**.

[7] K.S. Ngai, S. Ramesh, K. Ramesh, J.C. Juan, A review of polymer electrolytes: fundamental, approaches and applications, Ionics. 22 (2016) 1259-1279, **https://doi.org/10.1007/s11581-016-1756-4**.

[8] M. Abirami, R. Saratha, R. Shilpa, B. Vinitha, Preparation and characterization of Guar gum-based solid biopolymer electrolyte doped with lithium bis (trifluoromethanesulphonyl)imide (LiTFSI) plasticized with glycerol, Bull. Mater. Sci. 43 (2020) 254, **https://doi.org/10.1007/s12034-020-02218-z**.

[9] L. Liu, M. Li, M. Yu, M. Shen, Q. Wang, Y. Yu, J. Xie, Natural polysaccharides exhibit anti-tumor activity by targeting gut microbiota, Int. J. Biol. Macromol. 121 (2019) 743-751, **https://doi.org/10.1016/j.ijbiomac.2018.10.083**.

[10] X. Xu, P. Xu, C. Ma, J. Tang, X. Zhang, Gut microbiota, host health, and polysaccharides, Biotechnol. Adv. 31 (2012) 318-337, **https://doi.org/10.1016/). biotechadv.2012.12.009**.

[11] **S. Kalia, M.W. Sabaa, S. Kango, Polymer grafting: A versatile means to modify the polysaccharides, in: S. Kalia, M.W. Sabaa (Eds.), Polysaccharide Based Graft Copolymers, Springer, Berlin, Heidelberg, 2013, pp. 1-14**.

[12] G. Gopinath, S. Ayyasamy, P. Shanmugaraj, R. Swaminathan, K. Subbiah, S. Kandasamy, Effects of biopolymers in energy storage applications: a state-of-the-art review, J. Energy Storage 70 (2023) 108065, **https://doi.org/10.1016/). est.2023.108065**.

[13] **N.H. Muhamaruesaa, M.I.N.M. Isa, Biopolymer membranes for battery applications, in: M.A. de Moraes, C.F. da Silva, R.S. Vieira (Eds.), Biopolymer Membranes and Films Health, Food, Environment, and Energy Applications, Elsevier, 2020, pp. 477-500**.

[14] R. Ciriminna, N. Chavarría-Hernández, D.A.I. Rodriguez Hernández, M. Pagliaro, Pectin :a new perspective from the biorefinery standpoint, Biofpr (2015) 368-377, **https://doi.org/10.1002/bbb.1551**.

[15] J.R. Andrade, E. Raphael, A. Pawlicka, Plasticized pectin-based gel electrolytes, Electrochim. Acta 54 (2009) 6479-6483, **https://doi.org/10.1016/). electacta.2009.05.098**.

[16] V. Cyriac, I.M. Noor Ismayil, K. Mishra, C. Chavan, R.F. Bhajantri, S.P. Masti, Ionic conductivity enhancement of PVA: carboxymethyl cellulose poly-blend electrolyte films through the doping of NaI salt, Cellulose. 29 (2022) 3271-3291, **https://doi. org/10.1007/s10570-022-04483-z**.

[17] S.A. Hazaana, A. Joseph, S. Selvasekarapandian, R.M. Naachiyar, N.M. Vignesh, Performance of solid-state Li-ion conducting battery using biopolymer electrolyte based on agar-agar/lithium chloride, J. Solid State Electrochem. 27 (2022) 539-557, **https://doi.org/10.1007/s10008-022-05348-y**.

[18] M. Mahalakshmi, S. Selvanayagam, S. Selvasekarapandian, V. Moniha, R. Man)uladevi, P. Sangeetha, Characterization of biopolymer electrolytes based on cellulose acetate with magnesium perchlorate (Mg(ClO4)2) for energy storage devices, J. Sci. Adv. Mater. Dev. 4 (2019) 276-284, **https://doi.org/10.1016/). jsamd.2019.04.006**.

[19] M.A. Jothi, D. Vanitha, K. Sundaramahalingam, N. Nallamuthu, Utilisation of corn starch in production of 'eco friendly' polymer electrolytes for proton battery applications, Int. J. Hydrog. Energy 47 (2022) 28763-28772, **https://doi.org/ 10.1016/j.ijhydene.2022.06.192**.

[20] J.O. Dennis, A.A. Adam, M.K.M. Ali, H. Soleimani, M.F.B.A. Shukur, K.H. Ibnaouf, O. Aldaghri, M.H. Eisa, M.A. Ibrahem, A. Bashir Abdulkadir, V. Cyriac, Substantial proton ion conduction in methylcellulose/pectin/ammonium chloride based solid nanocomposite polymer electrolytes: effect of ZnO nanofiller, Membr. J. 12 (2022) 706, **https://doi.org/10.3390/membranes12070706**.

[21] A.F. Fuzlin, M.A. Saadiah, M.M. Hasan, Y. Nagao, I.I. Misnon, A.S. Samsudin, Involvement of ethylene carbonate on the enhancement H+ carriers in structural and ionic conduction performance on alginate bio-based polymer electrolytes, Int. J. Hydrog. Energy 47 (2022) 7846-7860, **https://doi.org/10.1016/). ijhydene.2021.12.124**.

[22] M.H. Hamsan, M.F. Zamani Kadir, M.F. Aziz, M.F. Shukur, Branched Glucan from Leuconostoc Mesenteroides as the channel for ionic migration in the fabrication of protonic (H+) battery, Int. J. Hydrog. Energy 47 (2022) 38690-38702, **https://doi. org/10.1016/j.ijhydene.2022.09.035**.

[23] A.A. Adam, H. Soleimani, M.F.B.A. Shukur, J.O. Dennis, Y.M. Hassan, B. A. Abdulkadir, J.Y. Yusuf, O.S.S. Ahmed, S.S. Salehan, S. Ayub, S.S. Abdullahi, Novel composite polymer electrolytes based on methylcellulose-pectin blend complexed with potassium phosphate and ethylene carbonate, Biomass Convers. Biorefin. (2022), **https://doi.org/10.1007/s13399-022-03202-9**.

[24] Y. Zouambia, K. Youcef Ettoumi, M. Krea, N. Moulai-Mostefa, A new approach for pectin extraction: electromagnetic induction heating, Arab. J. Chem. 10 (2017) 480-487, **https://doi.org/10.1016/j.arabjc.2014.11.011**.

[25] M.A. Saadiah, D. Zhang, Y. Nagao, S.K. Muzakir, A.S. Samsudin, Reducing crystallinity on thin film based CMC/PVA hybrid polymer for application as a host in polymer electrolytes, J. Non-Cryst. Solids 511 (2019) 201-211, **https://doi.org/ 10.1016/j.jnoncrysol.2018.11.032**.

[26] Y.H. Kim, R. Priyadarshi, J. Kim, J. Kim, D.G. Alekseev, J. Rhim, 3D-printed pectin/carboxymethyl cellulose/ZnO bio-inks: comparative analysis with the solution casting method, Polymers. 14 (2022) 4711, **https://doi.org/10.3390/ polym14214711**.

[27] S. Seslija, A. Nesiá, M.L. Skoric, M.K. Krusic, G. Santagata, M. Malinconico, Pectin/ carboxymethylcellulose films as a potential food packaging material, Macromol. Symp. 378 (2018) 1600163, **https://doi.org/10.1002/masy.201600163**.

[28] M. Muthukrishnan, C. Shanthi, S. Selvasekarapandian, G. Shanthi, L. Sampathkumar, T. Maheshwari, Impact of ammonium formate (AF) and ethylene carbonate (EC) on the structural, electrical, transport and electrochemical properties of pectin-based biopolymer membranes, Ionics. 27 (2021) 3443-3459, **https://doi.org/10.1007/s11581-021-04106-**.

[29] A.D. French, Idealized powder diffraction patterns for cellulose polymorphs, Cellulose. 21 (2014) 885-896, **https://doi.org/10.1007/s10570-013-0030-4**.

[30] E.M. de Melo, J.H. Clark, A.S. Matharu, The Hy-MASS concept: hydrothermal microwave assisted selective scissoring of cellulose for in situ production of (meso) porous nanocellulose fibrils and crystals, Green Chem. 14 (2017) 3408-3417, **https://doi.org/10.1039/C7GC01378G**.

[31] D. Panwar, P.S. Panesar, H.K. Chopra, Green extraction of pectin from Citrus limetta peels using organic acid and its characterization, Biomass Convers. Biorefin. (2021), **https://doi.org/10.1007/s13399-021-02127-z**.

[32] S. Selvalakshmi, T. Mathavan, S.S. Selvasekarapandian, M.M. Premalatha, Characterization of biodegradable solid polymer electrolyte system based on agar-NH4Br and its comparison with NH4I, J. Solid State Electrochem. 23 (2019) 1727-1737, **https://doi.org/10.1007/s10008-019-04262-0**.

[33] R.M. Hodge, G.H. Edward, G.P. Simon, Water absorption and states of water in semicrystalline poly(vinyl alcohol) films, Polymer. 37 (1996) 1371-1376, **https://doi.org/10.1016/0032-3861(96)81134-7**.

[34] W. Ren, F. Guo, J. Zhu, M. Cao, H. Wang, Yan Yu, A comparative study on the crystalline structure of cellulose isolated from bamboo fibers and parenchyma cells, Cellulose 28 (2021) 5993-6005, **https://doi.org/10.1007/s10570-021-03892-w**.

[35] R.K. Mishra, A.B.A. Majeed, A.K. Banthia, Development and characterization of pectin/gelatin hydrogel membranes for wound dressing, Int. J. Plast. Technol. 15 (2011) 82-95, **https://doi.org/10.1007/s12588-011-9016-y**.

[36] R.K. Mishra, M. Datt, A.K. Banthia, Synthesis and characterization of pectin/PVP hydrogel membranes for drug delivery system, AAPS PharmSciTech 9 (2008) 395-403, **https://doi.org/10.1208/s12249-008-9048-6**.

[37] T. Maheshwari, K. Tamilarasan, S. Selvasekarapandian, R. Chitra, M. Muthukrishnan, Synthesis and characterization of dextran, poly (vinyl alcohol) blend biopolymer electrolytes with NH4NO3, for electrochemical applications, Int. J. Green Energy 19 (2021) 314-320, **https://doi.org/10.1080/ 15435075.2021.1946811**.

[38] S.B. Aziz, M.M. Nofal, R.T. Abdulwahid, M.F.Z. Kadir, J.M. Hadi, M.M. Hessien, W. O. Kareem, E.M.A. Dannoun, S.R. Saeed, Impedance, FTIR and transport properties of plasticized proton

conducting biopolymer electrolyte based on chitosan for electrochemical device application, Results Phys. 29 (2021) 104770, **https://doi. org/10.1016/j.rinp.2021.104770**.

[39] M. Sangeetha, A. Mallikarjun, M. Jaipal Reddy, J. Siva Kumar, SEM, XRD and electrical conductivity studies of PVDF-HFP-LiBF4 -EC plasticized gel polymer electrolyte, AIP Conf. Proc. 1859 (2017) 020064, **https://doi.org/10.1063/ 1.4990217**.

[40] Y.L. Yap, A.H. You, L.L. Teo, Preparation and characterization studies of PMMA-PEO-blend solid polymer electrolytes with SiO2 filler and plasticizer for lithium ion battery, Ionics. 25 (2019) 3087-3098, **https://doi.org/10.1007/s11581-019-02842-8**.

[41] J.P. Sharma, K. Yamada, S.S. Sekhon, Conductivity study on PEO based polymer electrolytes containing hexafluorophosphate anion: effect of plasticizer, Macromol. Symp. 315 (2012) 188-197, **https://doi.org/10.1002/masy.201250523**.

[42] S. Das, A. Ghosh, Effect of plasticizers on ionic conductivity and dielectric relaxation of PEO-LiClO4 polymer electrolyte, Electrochim. Acta 171 (2015) 59-65, **https://doi.org/10.1016/j.electacta.2015.04.178**.

[43] S.K. Shetty, I.M. Noor Ismayil, Effect of new crystalline phase on the ionic conduction properties of sodium perchlorate salt doped carboxymethyl cellulose biopolymer electrolyte films, J. Polym. Res. 28 (2021) 415, **https://doi.org/ 10.1007/s10965-021-02781-x**.

[44] M. Muthukrishnan, C. Shanthi, S. Selvasekarapandian, R. Premkumar, Biodegradable flexible proton conducting solid biopolymer membranes based on pectin and ammonium salt for electrochemical applications, Int. J. Hydrog. Energy 48 (2023) 5387-5401, **https://doi.org/10.1016/j.ijhydene.2022.11.152**.

[45] T.M. Kanakaraj, R.F. Bhajantri, C. Chavan, V. Cyriac, S.S. Bulla, Ismayil, Investigation on the structural and ion transport properties of magnesium salt doped HPMC-PVA based polymer blend for energy storage applications, J. Non-Cryst. Solids 609 (2023) 122276, **https://doi.org/10.1016/j. jnoncrysol.2023.122276**.

[46] R.K. Prajapati, H. Kumar, A.L. Saroj, Formation of silver particles in [PVA:CS:PEG]-AgNO3 based biopolymer electrolyte membranes: Structural and electric transport properties study, Phys. B Condens. 662 (2023), 414962, **https://doi.org/10.1016/ j.physb.2023.414962**.

[47] Pritam, A. Arya, A.L. Sharma, Dielectric relaxations and transport properties parameter analysis of novel blended solid polymer electrolyte for sodium-ion rechargeable batteries, J. Mater. Sci. 54 (2019) 7131-7155, **https://doi.org/10.1007/s10853-019-03381-3**.

[48] E.M.A. Dannoun, S.B. Aziz, M.F.Z. Kadir, M.A. Brza, M.M. Nofal, J.M. Hadi, S.I. Al-Saeedi, R.T. Abdulwahid, The study of impedance, ion transport properties, EEC modelling, dielectric and electrochemical characteristics of plasticized proton conducting PVA based electrolytes, J. Mater. Res. Technol. 17 (2022) 1976-1985, **https://doi.org/10.1016/jjmrt.2022.01.152**.

[49] R.T. Abdulwahid, S.B. Aziz, M.F.Z. Kadir, Design of proton conducting solid biopolymer blend electrolytes based on chitosan-potato starch biopolymers: deep approaches to structural and ion relaxation dynamics of H + ion, J. Appl. Polym. Sci. 139 (2023), **https://doi.org/10.1002/app.52892 e52892**.

[50] A.K. Arof, S. Amirudin, S.Z. Yusof, I.M. Noor, A method based on impedance spectroscopy to determine transport properties of polymer electrolytes, Phys. Chem. Chem. Phys. 16 (2014) 1856-1867, **https://doi.org/10.1039/C3CP53830C**.

[51] N.F. Mazuki, M.Z. Kufian, Y. Nagao, A.S. Samsudin, Correlation studies between structural and ionic transport properties of lithium-ion hybrid gel polymer electrolytes based PMMA-PLA, J. Polym. Environ. 30 (2021) 1864-1879, **https:// doi.org/10.1007/s10924-021-02317-w**.

[52] N.A.M. Noor, M.I.N. Isa, Investigation on transport and thermal studies of solid polymer electrolyte based on carboxymethyl cellulose doped ammonium thiocyanate for potential application in electrochemical devices, Int. J. Hydrog. Energy 44 (2019) 8298-8306, **https://doi.org/10.1016/j.ijhydene.2019.02.062**.

[53] D.C. Bharati, P. Rawat, A.L. Saroj, Structural, thermal, and ion dynamics studies of PVA-CS-NaI-based biopolymer electrolyte films, J. Solid State Electrochem. 25 (2012) 1727-1741, **https://doi.org/10.1007/s10008-021-04946-6**.

[54] D. Kong, L.D. Wilson, Uptake of methylene blue from aqueous solution by pectin-chitosan binary composites, J. Compos. Sci. 4 (2020) 95, **https://doi.org/ 10.3390/jcs4030095**.

[55] N. Ajaz, I. Khalid, M.U. Minhas, K. Barkat, I.U. Khan, H.K. Syed, S. Asghar, R. Munir, F. Aslam, Pectin-based hydrogels with adjustable properties for controlled delivery of nifedipine: development and optimization, Polym. Bull. 77 (2019) 6063-6083, **https://doi.org/10.1007/s00289-019-03065-7**.

[56] V. Cyriac, I.S.B.M. Ismayil, Z.E. Noor, Y.N. Rojudi, C. Sudhakar, R.F. Bhajantri Chavan, M.S. Murari, Modification in the microstructure of sodium carboxymethylcellulose/polyvinyl alcohol polyblend films through the incorporation of NaNO 3 for energy storage applications, Int. J. Energy Res. 46 (2022) 22845-22866, **https://doi.org/10.1002/er.8588**.

[57] N.F. Mazuki, A.P.P. Abdul Majeed, Y. Nagao, A.S. Samsudin, Studies on ionics conduction properties of modification CMC-PVA based polymer blend electrolytes via impedance approach, Polym. Test. 81 (2020) 106234, **https://doi.org/ 10.1016/j.polymertesting.2019.106234**.

[58] H. Fan, Q. Wang, K. Li, Remarks on comments on effect of hydrolysed cellulose nanowhiskers on properties of montmorillonite/polylactic acid nanocomposites by Reza Arjmandi et al, Int. J. Biol. Macromol. 153 (2020) 676-679, **https://doi.org/ 10.1016/j.ijbiomac.2020.02.301**.

[59] S. Lin, G. Wu, Thermal degradation kinetics analysis of polymer composite electrolyte membranes of PEVOH and PBT nano fiber, Polymers. 14 (2022) 537, **https://doi.org/10.3390/polym14030537**.

[60] E.M. Abdelrazek, A.M. Abdelghany, S.I. Badr, M.A. Morsi, Structural, optical, morphological and thermal properties of PEO/PVP blend containing different concentrations of biosynthesized Au nanoparticles, J. Mater. Res. Technol. 7 (2018) 419-431, **https://doi.org/10.1016/jjmrt.2017.06.009**.

[61] S. Ibrahim, S.M.M. Yasin, R. Ahmad, M.R. Johan, Effects of various EC plasticizer concentrations on salted PEO based solid polymer electrolytes, Int. J. Plast. Technol. 16 (2012) 125-135, **https://doi.org/10.1007/s12588-012-9034**.

[62] A.R. Polu, R. Kumar, Preparation and characterization of pva based solid polymer electrolytes for electrochemical cell applications, Chin. J. Polym. Sci. 31 (2013) 641-648, **https://doi.org/10.1007/s10118-013-1246-3**.

[63] G.K. Prajapati, R. Roshan, P.N. Gupta, Effect of plasticizer on ionic transport and dielectric properties of PVA-H3PO4 proton conducting polymeric electrolytes, J. Phys. Chem. Solids 71 (2010) 1717-1723, **https://doi.org/10.1016Zj. jpcs.2010.08.023**.

[64] K. Maithilee, P. Sathya, S. Selvasekarapandian, R. Chitra, S. Meyvel, Investigation on tamarind seed polysaccharide biopolymer electrolyte doped with sodium nitrite and EC plasticizer for primary sodium battery, Bull. Mater. Sci. 46 (2023) 114, **https://doi.org/10.1007/s12034-023-02948-w**.

[65] S. Selvalakshmi, N. Vijaya, S. Selvasekarapandian, M. Premalatha, Biopolymer agar-agar doped with NH sub(4)SCN as solid polymer electrolyte for electrochemical cell application, J. Appl. Polym. Sci. 134 (2017) 44702, **https:// doi.org/10.1002/app.44702**.

[66] S. Rudhziah, A. Ahmad, I. Ahmad, N.S. Mohamed, Biopolymer electrolytes based on blend of kappa-carrageenan and cellulose derivatives for potential application in dye sensitized solar cell, Electrochim. Acta 175 (2015) 162-168, **https://doi. org/10.1016/j.electacta.2015.02.153**.

[67] S.B. Aziz, E.M.A. Dannoun, M.A. Brza, N.M. Sadiq, M.M. Nofal, W.O. Karim, S.I. Al-Saeedi, M.F.Z. Kadir, An investigation into the PVA:MC:NH4Cl-based protonconducting polymer-blend electrolytes for electrochemical double layer capacitor (EDLC) device application: the FTIR, circuit design and electrochemical studies, Molecules. 27 (2022) 1011, **https://doi.org/10.3390/molecules27031011**.

[68] M.F.Z. Kadir, A.K. Arof, Application of PVA-chitosan blend polymer electrolyte membrane in electrical double layer capacitor, Mater. Res. Innov. 12 (2013) s217-s220, **https://doi.org/10.1179/143307511X13031890749299**.

[69] B. Xia, B. Ye, J. Cao, Polarization voltage characterization of lithium-ion batteries based on a lumped diffusion model and joint parameter estimation algorithm, Energies. 15 (2022) 1150, **https://doi.org/10.3390/en15031150**.

[70] P. Nayak, V. Cyriac Ismayil, S. Hegde, G. Sanjeev, M.S. Murari, Y.N. Sudhakar, Magnesium ion conducting free-standing biopolymer blend electrolyte films for electrochemical device application, J. Non-Cryst. Solids 592 (2022) 121741, **https://doi.org/10.1016/jjnoncrysol.2022.121741**.

[71] M. Vahini, M. Muthuvinayagam, M.I.N. Isa, Preparation and characterization of biopolymer electrolytes based on pectin and NaNO3 for battery applications, Polym. Sci. Ser. A 61 (2019) 823-831, **https://doi.org/10.1134/ S0965545X19060129**.